

1

Microelectromechanical Systems (MEMS)

1.1 INTRODUCTION

Microelectromechanical systems (MEMS) refer to a collection of microsecond and actuators that can sense its environment and have the ability to react to changes in that environment with the use of a microcircuit control. They include, in addition to the conventional microelectronics packaging, integrating antenna structures for command signals into microelectromechanical structures for desired sensing and actuating functions. The system may also need micropower supply, microrelay, and microsignal processing units. Microcomponents make the system faster, more reliable, cheaper, and capable of incorporating more complex functions.

In the beginning of 1990s, MEMS emerged with the aid of the development of integrated circuit (IC) fabrication processes, in which sensors, actuators, and control functions are cofabricated in silicon. Since then, remarkable research progresses have been achieved in MEMS under the strong capital promotions from both government and industries. In addition to the commercialization of some less-integrated MEMS devices, such as microaccelerometers, inkjet printer head, micromirrors for projection, etc., the concepts and feasibility of more complex MEMS devices have been proposed and demonstrated for the applications in such varied fields as microfluidics, aerospace, biomedical, chemical analysis, wireless communications, data storage, display, optics, etc [1,2]. Some branches of MEMS, appearing as microoptoelectromechanical systems (MOEMS), micro-total analysis systems (μ TAS), etc., have attracted a great deal of research interests since their potential applications' market. As of the

end of 1990s, most of MEMS devices with various sensing or actuating mechanisms were fabricated using silicon bulk micromachining, surface micromachining, and lithography, galvanofforming, moulding (LIGA) processes [3–5]. Three-dimensional (3D) microfabrication processes incorporating more materials were presented for MEMS recently, when some specific application requirements (e.g., Biomedical devices) and the microactuators with higher output power were called for in MEMS [1,5–11].

Micromachining has become the fundamental technology for the fabrication of microelectromechanical devices and, in particular, miniaturized sensors and actuators. Silicon micromachining is the most advanced of the micromachining technologies, and it allows for the fabrication of MEMS that have dimensions in the submillimeter range. It refers to fashioning microscopic mechanical parts out of silicon substrate or on a silicon substrate, making the structures three dimensional and bringing new principles to the designers. Employing materials such as crystalline silicon, polycrystalline silicon, silicon nitride, etc., a variety of mechanical microstructures including beams, diaphragms, grooves, orifices, springs, gears, suspensions, and a great diversity of other complex mechanical structures have been conceived [12–16].

Sometimes many microdevices can also be fabricated using semiconductor processing technologies or stereolithography on the polymeric multifunctional structures. Stereolithography is a poor man's LIGA for fabricating high aspect ratio MEMS devices in UV-curable semiconducting polymers. With proper doping, a semiconducting polymer structure can be synthesized, and using stereolithography, it is now possible to make 3D microstructure of high aspect ratio. Ikuta et al., [8] demonstrated that a 3D microstructure of polymers and metal is feasible using a process named *IH Process* (integrated harden polymer stereolithography). Using UV light source, XYZ-stage, shutter, lens, and microcomputer, it has been shown that microdevices such as spring, venous valve, and electrostatic microactuator can be fabricated. In case of difficulty with polymeric materials, some of these devices can be micromachined in silicon, and the system architecture can be obtained by photoforming or hybrid processing [7–9,17–19]. The photoforming or photofabrication is an optical method such as stereolithography, photomask-layering process, and IH process that involve solidification of photochemical resin by light exposure. Takagi and Nakajima [9] proposed new concepts of 'combined architecture' and 'glue mechanism' using the photoforming process to fabricate complicated structures by combining components, each of them made by its best fabrication

process. Batch processing of such hybrid silicon and polymer devices thus seems feasible.

The combined architecture may also result in sheets of smart skin with integrated sensors and actuators at the μm -to- mm scale. For some applications (say airfoil surface), the smart skin substrate has to be flexible to conform to the airfoil shape, and at the same time it has to be compatible with the integrated circuit (IC) processing for sensor and smart electronics integration. It has been proposed by Carraway [20] that polyimide is an excellent material for use as the skin because of its flexibility and IC processing compatibility. The control loop between the sensors and actuators employs the multifunctional materials that provide electrical functionality at selected locations using conductive polymers and electrodes that are connected to on-site antennas communicating with a central antenna. A related and difficult problem, and one that has been largely unaddressed, is the method for telemetry of the data. In some applications, stresses and strains to which the structure is subjected to may pose a problem for conventional cabling. In others, environmental effects may affect system performance. Advances in ultra flat antenna technology coupled with MEMS sensors and actuators seem to be an efficient solution. The integration of micromachining and microelectronics on one chip results in so-called smart sensors. In smart sensors, small sensor signals are amplified, conditioned, and transformed into a standard output format. They may include microcontroller, digital signal processor, application-specific integrated circuit (ASIC), self-test, self-calibration, and bus interface circuits simplifying their use and making them more accurate and reliable.

The basic MEMS use a diaphragm-based, a microbridge-based, or a cantilever-based structure. Special processing steps commonly known as *micromachining* are needed to fabricate these membranes, cantilever beams, resonant structures, etc., that are discussed later. For a given application, it may be necessary to have integrated MEMS employing one or more of the basic structure. These three structures provide some feasible designs for microsecond and actuators that eventually perform the desired task in most of smart structures. However, the main issues with respect to implementing these structures are the choice of materials that are to be used in fabricating these devices and the micromachining technology that may be used. To address the first issue, we note that in all of the three structures proposed, the sensing and actuation occur as a result of exciting a piezoelectric layer by the application of an electric field. This excitation brings about sensing and actuation in the form of expansion in the diaphragm, in the free-standing beam in the

microbridge structure, or in the cantilever beam. In the former two cases the expansion translates into upward curvature in the diaphragm or in the free-standing beam, thus, resulting in a net vertical displacement from the unexcited equilibrium configuration. In the cantilever case, however, and upon the application of electric field, the actuation occurs by a vertical upward movement of the cantilever tip. Evidently in all three designs the material system structure of the active part (diaphragm, free-standing beam, or cantilever beam) in the microactuator must comprise at least one piezoelectric layer and conducting electrodes for the application of electric field across this layer. Piezoelectric force is used for actuation for many of the applications mentioned earlier. Micromachining is employed to fabricate the membranes, cantilever beams, and resonant structures.

Microsensors and actuators are fabricated using the well-known micromachining techniques in microelectronics industry. Three-dimensional microactuators in polymer structures can be achieved using stereolithography on UV-curable backbone-type polymers [7–9,17–19]. In the integrated MEMS device, we may use photoforming processing in achieving the combined sensor and actuator architecture as outlined by Takagi and Nakajima [9]. For large actuation, one could use a flex tensional transducer consisting of a piezoelectric diaphragm bridged into a cavity [21].

Silicon micromachining has been a key factor for the vast progress of MEMS in the last decade. This refers to the fashioning of microscopic mechanical parts out of silicon substrates and, more recently, other materials. It is used to fabricate such features as clamped beams, membranes, cantilevers, grooves, orifices, springs, gears, suspensions, etc. These can be assembled to create a variety of sensors. **Recently, the Japanese exhibited a complete functioning micromachined automobile that operated for several minutes. Bulk micromachining is the commonly used method, but it is being replaced by surface micromachining that offers the attractive possibility of integrating the machined device with microelectronics that can be patterned and assembled on the same wafer. Thus power supply circuitry and signal processing using ASICs can be incorporated. It is the efficiency of creating several such complete packages using existing technology that makes this an attractive approach.**

1.2 MICROFABRICATIONS FOR MEMS

Silicon micromachining has been a key factor for the vast progress of MEMS. Silicon micromachining refers to fashioning microscopic

mechanical parts out of a silicon substrate or on a silicon substrate. Silicon micromachining comprises two technologies: bulk micromachining, in which structures are etched into silicon substrate and surface micromachining, in which the micromechanical layers are formed from layers and films deposited on the surface.

Bulk micromachining and surface micromachining are the two major micromachining processes of silicon, and silicon wafer bonding is usually necessary for silicon microfabrication. LIGA and 3D microfabrications have been used for high aspect ratio and 3D-microstructure fabrication for MEMS.

1.2.1 Bulk Micromachining of Silicon

Bulk micromachining is one of the most popular silicon micromachining technologies. It emerged in the early 1960s and has been used since then in the fabrication of different microstructures. It is used in the manufacturing of majority of commercial devices: almost all of pressure sensors and silicon valves and 90 percent of silicon accelerometers. The term *bulk micromachining* comes from the fact that this type of micromachining is used to realize micromechanical structures within the bulk of a single-crystal silicon wafer by selectively removing ('etching') wafer material. The microstructures fabricated using bulk micromachining may cover the thickness range from submicron to full wafer thickness (200–500 μm), and the lateral size range from submicron to the lateral dimensions of a full wafer. Bulk micromachining technique allows to selectively remove significant amounts of silicon from a substrate to form membranes on one side of a wafer, a variety of trenches, holes, or other structures (Figure 1.1). Bulk micromachining technique can be divided into wet etching and dry etching of silicon according to the phase of etchants. Liquid etchants, almost exclusively relying on aqueous chemicals, are referred to as *wet etching*. Vapor and plasma etchants are referred to as *dry etching*.

For etching such thick silicon substrate, anisotropic wet etchants such as solutions of potassium hydroxide (KOH), ethylene diamine and pyrocatechol (EDP), tetramethylammonium hydroxide (TMAH), and hydrazine-water are used. These etchants have different etch rates in different crystal orientation of the silicon [13,22]. Wet etching in most case is done from the back side of the wafer while the plasma etching is being applied to front side. In recent years, a vertical-walled bulk micromachining technique known as *SCREAM*, which is a combination

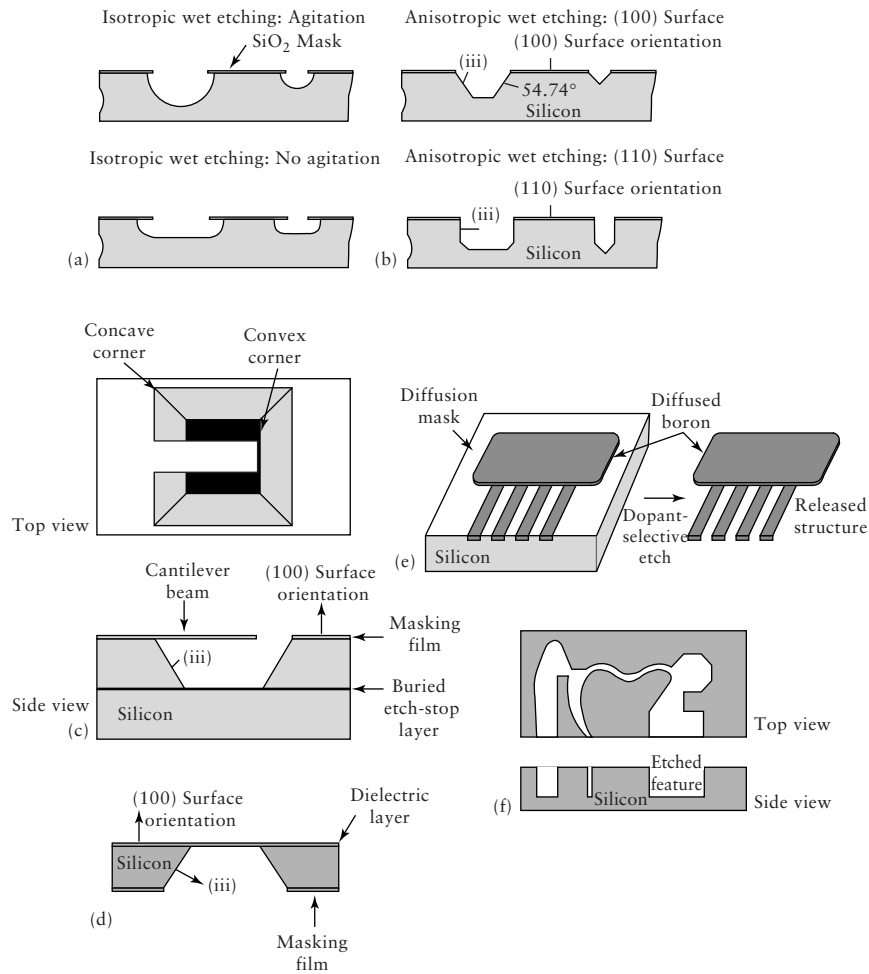


Figure 1.1 Bulk silicon micromachining. (a) Isotropical etching, (b) Anisotropic etching, (c) Anisotropic etching with buried etch-stop layer, (d) Dielectric membrane released by back-side bulk etching, (e) Dopant-dependant wet etching, (f) Anisotropic dry etching [3]

of anisotropic and isotropic plasma etching, is used [23]. Etch process can be made selective by the use of dopants (heavily doped regions etch slowly) or may even be halted electrochemically (e.g., etching stops upon encountering a region of different polarity in a biased p–n junction). A region at which wet etching tends to slow down or diminish is called an *etch-stop*. There are several ways in which an etch-stop region

can be created: doping-selective etching (DSE) and bias-dependent DSE [13,22,23].

Wet etching occurs by dipping substrate into an etching bath or spraying it with etchants that may be acid or alkaline. Wet etching can either be isotropic etching or anisotropic etching depending on the structure of the materials or the etchants used. If the material is amorphous or polycrystalline, wet etching is always isotropic etching (Figure 1.1a). During isotropic etching (etchants used are acid solution), resist is always undercut, implying that the deep etching is not practical for MEMS. Single-crystal silicon can be anisotropically etched. The etching features are determined by the etching speed that is dependent on the crystal's orientation. The etching slows down significantly at the (111) planes of silicon, relative to other planes. With the chosen wafers with different crystal orientation, different bulk machined features can be achieved (Figure 1.1b,c). Most common etchants used for anisotropic etching of silicon include alkali hydroxide etchants (KOH, NaOH, etc.), ammonium-based solutions (NH₄OH, TMAH ((CH₃)₄NOH), etc.), and EDP (ethylene diamine, pyrochatechol, and water). By combining anisotropic etching with boron implantation (P+ etch-stop) and electrochemical etch-stop technique, varied silicon microstructures can be bulk machined (Figure 1.1d,e).

Dry etching occurs through chemical or physical interaction between the ions in the gas and the atoms of the substrate. The nonplasma, isotropic dry etching is possible using xenon difluoride or a mixture of interhalogen gases and provides very high selectivity for aluminum, silicon dioxide, silicon nitride, photoresist, etc. The most common dry etching of bulk silicon are plasma etching and reactive ion etching (RIE), in which the external energy in the form of radio frequency (RF) power drives chemical reactions in low-pressure reaction chambers. A wide variety of chlorofluorocarbon gases, sulfur hexafluoride, bromine compounds, and oxygen are commonly used as reactants. The anisotropic dry etching processes are widely used in MEMS because of the geometry flexibility and the less chemical contamination as compared with wet etching. An arbitrarily oriented feature etched deep into silicon using the anisotropic dry etching (Figure 1.1f). Very deep silicon microstructures can be obtained by the deep RIE (DRIE) dry etching [14].

With bulk-micromachined silicon microstructures, the wafer-bonding technique is necessary for the assembled MEMS devices. The surface micromachining, however, can be used to build the monolithic MEMS devices.

1.2.2 Surface Micromachining of Silicon

Surface micromachining does not shape the bulk silicon but instead builds structures on the surface of the silicon by depositing thin films of ‘sacrificial layers’ and ‘structural layers’ and by removing eventually the sacrificial layers to release the mechanical structures (Figure 1.2). The dimensions of these surface micromachined structures can be several orders of magnitude smaller than bulk-micromachined structures. The prime advantage of surface-micromachined structures is their easy integration with IC components, because the wafer is also the working area for IC elements. It should be noted that as miniaturization is immensely increased by surface micromachining, the small mass structure involved may be insufficient for a number of mechanical sensing and actuation applications.

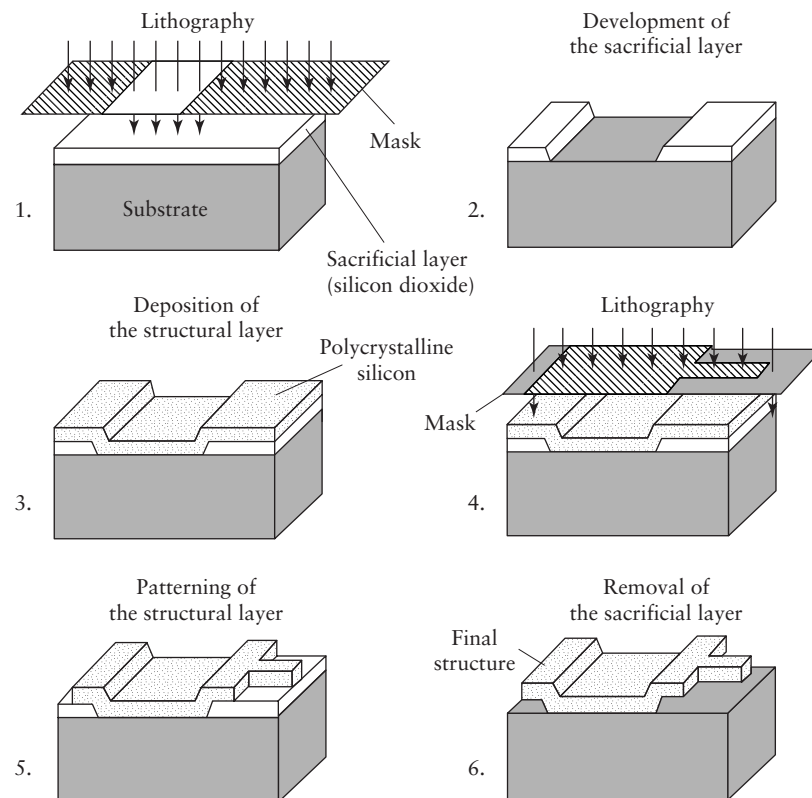


Figure 1.2 Processing steps of typical surface micromachining [24]

Surface micromachining requires a compatible set of structural materials, sacrificial materials, and chemical etchants. The structural materials must possess the physical and chemical properties that are suitable for the desired application. In addition, they must have satisfactory mechanical properties, for e.g., high yield and fracture stresses, minimal creep and fatigue, and good wear resistance. The sacrificial materials must have good mechanical properties to avoid device failure during fabrication. These properties include good adhesion and low-residual stresses to eliminate device failure by delamination and/or cracking. The etchants to remove the sacrificial materials must have excellent etch selectivity and they must be able to etch off the sacrificial materials without affecting the structural ones. In addition, the etchants must have proper viscosity and surface tension characteristics. The common IC compatible materials used in surface micromachining are

- 1 Poly-Si/Silicon dioxide; low-pressure chemical vapor deposition (LPCVD)-deposited poly-Si as the structural material and LPCVD deposited oxide as the sacrificial material. The oxide is readily dissolved in HF solution without the poly-Si being affected. Together with this material system, silicon nitride is often used for electrical insulation
- 2 Polyimide/aluminum; in this case polyimide is the structural material and aluminum is the sacrificial material. Acid-based etchants are used to dissolve the aluminum sacrificial layer
- 3 Silicon Nitride/poly-Si; Silicon Nitride is used as the structural material, whereas poly-Si is the sacrificial material. For this material system, silicon anisotropic etchants such as KOH and EDP are used to dissolve poly-Si, and
- 4 Tungsten/Silicon Dioxide; chemical vapor deposition (CVD)-deposited tungsten is used as the structural material with oxide as the sacrificial material. HF solution is used to remove the sacrificial oxide. Other IC compatible materials such as silicon carbide, diamond-like carbon, zinc oxide, gold, etc., are also used.

Surface micromachining could also be performed using dry etching methods. Plasma etching of the silicon substrate with SF₆/O₂-based and CF₄/H₂-based gas mixtures is advantageous because high selectivities for photoresist, silicon dioxide, and aluminum masks can be achieved. However, when using plasma etching, a large undercut of the mask is observed. This is due to the isotropic fluorine atom etching of silicon that is known to be high compared with the vertical etch induced by

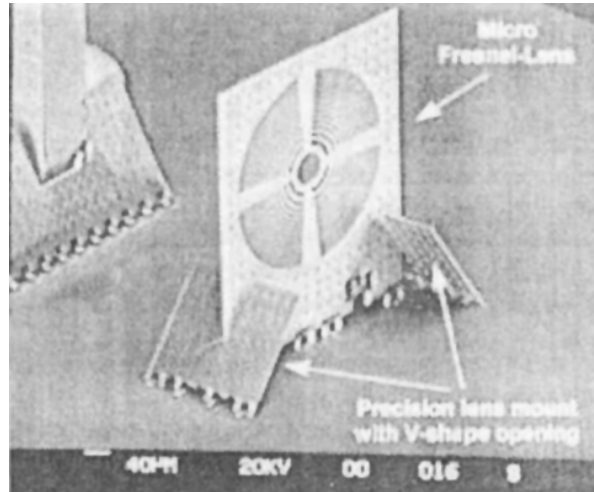


Figure 1.3 SEM of a Fresnel lens by modified surface micromachining [90]

ion bombardment. In contrast, reactive ion etching of poly-Si using chlorine–fluorine gas combination produces virtually no undercut and almost vertical etch profiles when using photoresist as a masking material. Thus rectangular silicon patterns that are up to 30 μm deep can be formed using chlorine–fluorine plasmas out of poly-Si films and the Si wafer surface.

Silicon microstructures fabricated by surface micromachining are usually planar structures (or two-dimensional). Other techniques involving the use of thin film structural materials released by the removal of an underlying sacrificial layer have helped to extend conventional surface micromachining into the third dimension. By connecting polysilicon plates to the substrate and to each other with hinges, 3D micromechanical structures can be assembled after release. Another approach to 3D structures used the conformal deposition of polysilicon and sacrificial oxide films to fill deep trenches previously etched in the silicon substrate. An example of the 3D-micromechanical structures fabricated using modified surface micromachining process is shown in Figure 1.3. These 3D microstructures are especially useful for optical microdevices without the requirement for contact power output.

1.2.3 Wafer Bonding for MEMS

Silicon micromachining has limitations in forming complex 3D microstructures in a monolithic format; multichip structures are then

proposed for advanced MEMS, in which wafer-to-wafer bonding is critical in the formation [25].

The wafer bonding for MEMS can be categorized into three major types: anodic bonding, intermediate-layer bonding-assisted bonding, and direct bonding.

Anodic Bonding

Anodic bonding is also called *field-assisted thermal bonding*, *electrostatic bonding*, etc. Anodic bonding is usually established between a sodium glass and silicon for MEMS. For the anodic bonding, a cathode and an anode are attached to the glass (or silicon with glass thin coating) and silicon wafer, respectively, and voltages applied ranged from 200 to 1000 V. At the same time, the anode is put on a heater providing the bonding temperature around 180 ~ 500 °C (Figure 1.4). During the bonding, oxygen ions from the glass migrate into the silicon resulting in the formation of silicon dioxide layer between silicon wafer and glass wafer and form a strong and hermetic chemical bond.

The advantage of anodic bonding for MEMS is that the low temperature used can ensure the metalization layer (aluminum) to withstand this temperature without degradation.

Intermediate Layer-Assisted Bonding

This type of bonding for MEMS requires an intermediate layer, which can be metal, polymer, solders, glasses, etc., to fulfill the bonding between wafers [25].

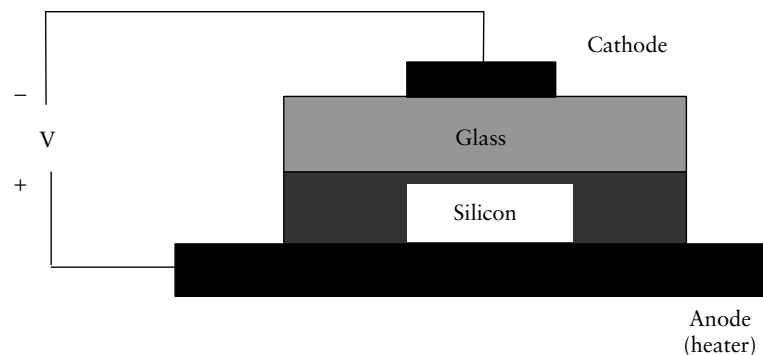


Figure 1.4 Anodic bonding

One of the earliest wafer bonding, that is, eutectic bonding used Au as the intermediate layer for Si–Si bonding for pressure sensor [26]. The Au–Si eutectic bonding takes place at 363 °C, well below the critical temperature of metallized Al layer. But the stress generated during bonding was found significant and introduced the sensor drift [26].

Polymers as intermediate layer for bonding prevail in very low temperature, reasonable high strength, absence of metal ions, low stress due to the elastic property of polymers, etc. Usually, UV photoresists such as polyimide, AZ-4000, SU-8, poly(methyl methacrylate) (PMMA), and other UV-curable cross-linked polymers [27]. The disadvantage is that the bonded device with polymer may not hold the hermetic sealing performance because of the relatively high permittivity of polymers.

Glasses with low melting temperature as intermediate layer for the bonding, in which a layer of glass frit is usually deposited on the silicon wafer, are also demonstrated. The flatness of the deposited frit layer is critical to obtain uniform, strong, and low-stress bonding. The screen printing of glass frit was used for pressure-sensor bonding and it exhibited good performance [26].

Other materials are also developed as the intermediate layer for bonding with low temperature, high strength, and low stress [25].

Direct Bonding

Direct bonding is also called *silicon fusion bonding*, which is used for silicon–silicon bonding. Direct bonding is based on a chemical reaction between OH-groups present at the surface of native silicon or grown oxides covering the wafers [27]. The direct bonding usually follows three steps: surface preparation, contacting, and thermal annealing.

The surface preparation step involves cleaning the surfaces of the two wafers to form a hydrate surface. The wafer surface should be mirror smooth, the roughness should be no greater than 10 Å, and the bow of a 4" wafer should be less than 5 micron to achieve the necessary flatness [25]. Following this preparation, the wafers are aligned and contacted in a clean room environment by gently pressing the two wafers at the surface central point. The surface attraction of the two hydrated surfaces then brings the intimate contact over the entire wafer surfaces. The final step in direct bonding is to anneal the bonding from the room temperature to 1200 °C. This anneal process increases the bond strength by more than one order of magnitude at temperatures as high as 800 ~ 1200 °C. But the high-temperature annealing is not allowed for the metallized wafers. In

comparison to anodic bonding, relatively high-strength bonding could be achieved by using direct bonding with high-temperature annealing [26]. Some low-temperature direct-bonding processes are to be further developed.

1.2.4 LIGA Process

MEMS generally require complex microstructures that are thick and three-dimensional [2]. Therefore, many microfabrication technologies have been developed to achieve high-aspect-ratio (height-to-width) and 3D devices. LIGA process is one of those microfabrications.

LIGA is a German acronym for Lithographie, Galvanoformung, Abformung (lithography, galvanofforming, molding). It was developed by the research Center Karlsruhe in the early 1980s in Germany using X-ray lithography for mask exposure, galvanofforming to form the metallic parts, and molding to produce microparts with plastic, metal, ceramics, or their combinations [5]. A schematic diagram of the LIGA process is shown in Figure 1.5. With the LIGA process, microstructure's height can be up to hundreds of microns to millimeter scale, while the lateral resolution is kept at submicron because of the advanced X-ray lithography. Various materials can be incorporated into LIGA process allowing electric, magnetic, piezoelectric, optic, and insulating properties of sensors and actuators with a high-aspect ratio, which are not possible to make with the silicon-based processes. Besides, by combining the sacrificial layer technique and LIGA process, advanced MEMS with moveable microstructures can be built (Figure 1.6). However, the high production cost of LIGA process because of the fact that it is not easy to access X-ray source limits the application of LIGA. Another disadvantage of LIGA process relies on the fact that structures fabricated using LIGA are not truly three dimensional, because the third dimension is always in a straight feature. As we know that complex thick 3D structures are necessary for some advanced MEMS, it means that other 3D-microfabrication processes need to be developed for MEMS.

1.2.5 Micromachining of Polymeric MEMS Devices

In the micromachining concept for polymeric MEMS devices, two types of polymers are employed: one is the structural polymer and the other one is a sacrificial polymer. The structural polymer is usually an UV-curable polymer with urethane acrylate, epoxy acrylate, and acryloxysilane as

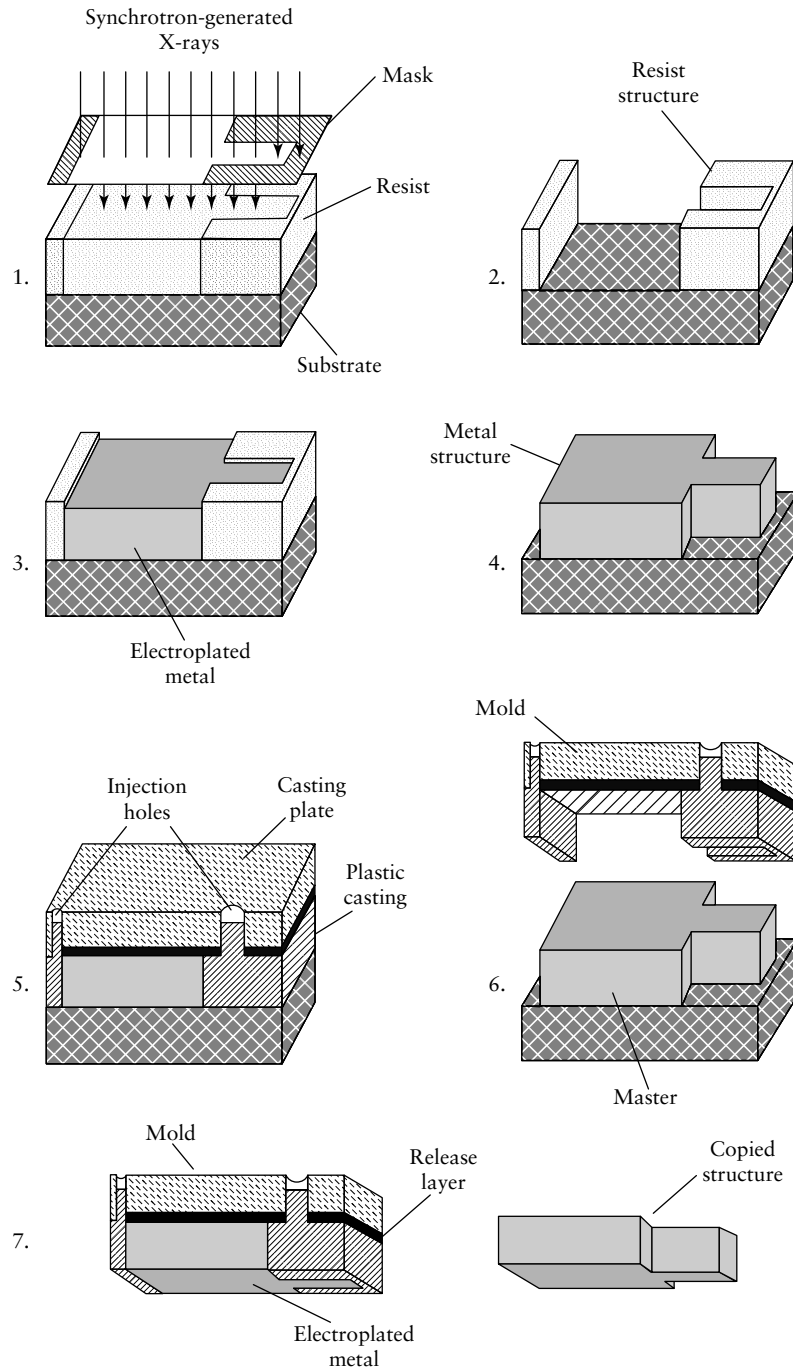


Figure 1.5 LIGA process [24]

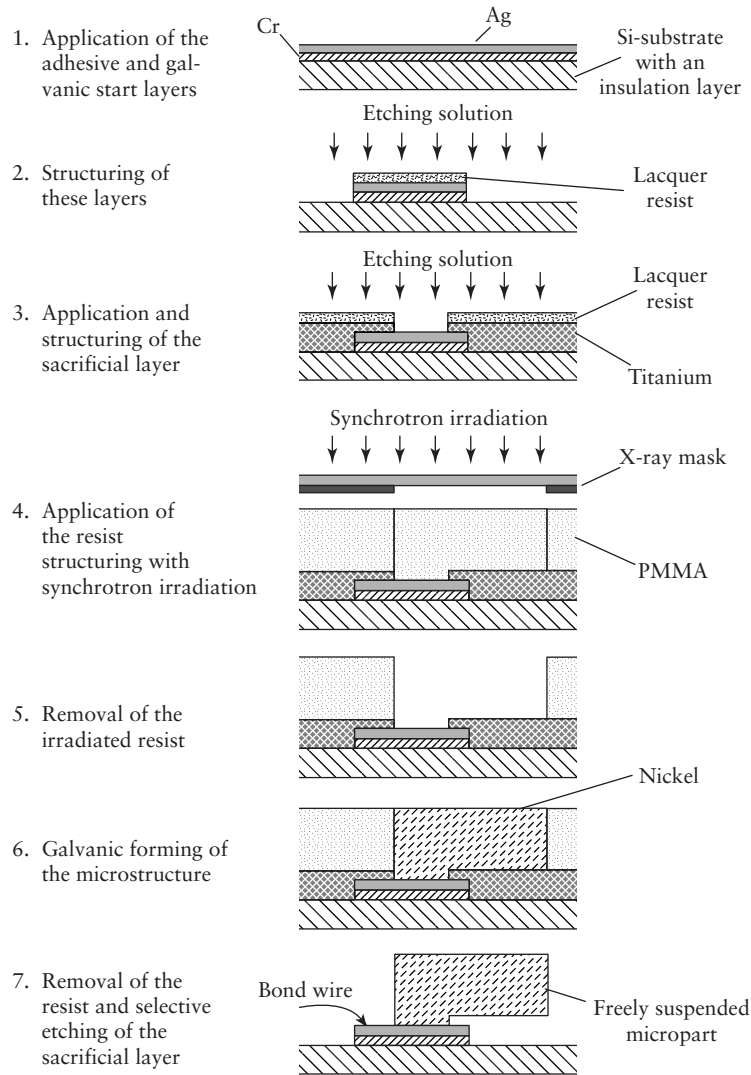


Figure 1.6 Combination of LIGA process and sacrificial layer process [28]

main ingredients. Its low viscosity allows easy processing through automatic equipment or manual methods without the addition of solvents or heat to reduce the viscosity. It also complies with all VOC regulations. It has excellent flexibility and resistance to fungus, solvents, water, and chemicals. Other physical, chemical, mechanical, and thermal properties are given in Table 1.1 (HVS Technologies, State College, PA 16803). This structural polymer may be used as a backbone structure

Table 1.1 General properties of polymer

Physical properties	
Clarity	Transparent
Flexibility	Good
Adhesion (#600 Cellotape)	Excellent
Weather Resistance	Excellent
Flammability, ASTM D635	Self-extinguishing
Chemical properties	
Fungus resistance, ASTM-G21	Excellent
Resistance to solvents	Excellent
Resistance to chemicals	Excellent
Resistance to water	Excellent
Thermal properties	
Continuous operating range 0 °C	65 to 125
Decomposition temperature	242
Mechanical properties	
Tensile Strength (psi), ASTM D 683	3454
Percentage elongation, ASTM D 683	5.2
Dielectric properties	
Dielectric permittivity (200–1000 MHz)	1.9–2.0
Loss tangent (200–1000 MHz)	0.023–0.05

for building the multifunctional polymer described in the following section.

For 3D MEMS devices, the polymers need to have conductive and possibly piezoelectric or ferroelectric properties. For these polymers to be used for polymeric MEMS, they have to meet the following requirements:

- 1 Interactions (chemical or physical) between functional polymer and nanoceramics
- 2 Strong interfacial adhesion between functional polymer and conducting polymer layers
- 3 Suitable elastic moduli to support the deformation initiated by MEMS devices
- 4 Excellent overall dimension stability (allowing local mobility)
- 5 Processes conducive to the attachment of nanoceramics and/or conductive phases and formation of a uniform coating layer and
- 6 Long-term environmental stability.

In addition, the multifunctionality of these polymers provides a large-scale strain under electric field, and thus can be used as actuators for

MEMS-based devices such as micropumps. In general, these polymers are biocompatible and are thus useful for many medical devices. Other applications may include implanted medical delivery systems, chemical and biological instruments, fluid delivery in engines, pump coolants, and refrigerants for local cooling of electronic components. The sacrificial polymer is an acrylic resin containing 50 percent silica and is modified by adding Crystal Violet [16]. This composition is UV-curable and can be dissolved with 2 Mol/L caustic soda at 80 °C. In principle, this process is similar to the surface micromachining used for silicon devices. However, the process yields 3D structures.

1.2.6 3D Microfabrications

To fabricate 3D structures for MEMS, many novel 3D-microfabrication techniques have been developed. Among them, microscale free-form fabrications are very impressive to achieve the 3D-MEMS devices.

Most of the free-form fabrications build 3D microstructures in an additive layer by layer fashion (Figure 1.7). The members of the free-form microfabrication's family include microstereolithography [8], electrochemical fabrication (EFAB) [29], microphotoforming [9], spatial forming [10], microtransfer molding [6], localized electrochemical deposition [30], etc. Complex 3D microstructures have been built using these techniques from the materials of polymer, ceramic, metal, etc. In principle, other smart materials can be incorporated into these microfabrications.

Another approach to build 3D MEMS devices is to combine the current micromachining processes, such as silicon micromachining, LIGA, precision mechanical machining, etc., or to combine the new 3D-microfabrication processes with the silicon micromachining and LIGA processes [31,32]. AMANDA process is one of these combined microfabrication processes, which combined LIGA process (or precision machining) with silicon micromachining. AMANDA

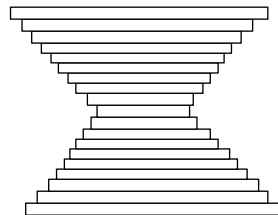


Figure 1.7 Free-form 3D microfabrication (additive)

is the German acronym for *Abforming, Oberflächenmikromechanik und Membranübertragung*. The English translation could be surface micromachining, molding, and diaphragm transfer. AMANDA process is especially powerful in polymer MEMS fabrication [33].

It is known that 3D MEMS devices are usually with multiple layers fabricated from many different structural and functional materials. At the beginning of MEMS fabrications, silicon and polysilicon are the major structural materials, but more structural materials need to be incorporated into MEMS devices as largely diverged applications require varied properties from the microstructures. For example, for the bio-MEMS devices, structural materials should be biocompatible. Many polymers are then selected and used to build structures [34]. Although refractory materials may be required for the structures used in high temperature, harsh environment, etc., structural ceramics may be the first choice for this type of applications [35,36]. Metallic structures have a good reputation in the macroworld, however, some of the properties of metals are still maintained in microscale. Therefore, 3D microfabrications capable of processing a broad spectrum of structural materials were expected for MEMS, and many progresses have been made [8–10,29,37,38].

On the other hand, most of the sensing and actuating structures used in MEMS were fabricated from thin films. For microseconds, it is advantageous to use the microelectronic's compatible processes. But actuators are devices that modify their environment; they are fundamentally 3D devices [5]. Thick and 3D structures are advantageous to provide higher output power, which has been expected for a while for MEMS, as low-power output MEMS are less significant in actuation so far. So, incorporating more smart materials into MEMS devices acting as sensing and actuating structures has become the concern in MEMS development.

For 3D MEMS devices, the polymers need to have conductive and possibly piezo or ferroelectric properties. Such MEMS polymers involve the integration of conventional UV-curable polymers, optically transparent conductive polymers, and nano-piezo or ferroelectric particles by chemical bonding as side groups on the polymer backbone. The concept is to design a backbone with functional groups that will serve as anchor points for the metal oxides. The nanoparticles such as PZT, (lead, zirconium, titanate) PLZT, (lead, lanthanum, zirconium, titanate) etc. must have active surfaces or functional groups that can bond with the polymer chain. The nanoparticles provide the piezoelectric function in the polymer, and the backbone provides the mechanical stability and flexibility if it is needed.

1.3 MICROSENSING AND MICROACTUATION FOR MEMS

Various microsensing and microactuation mechanisms have been developed for MEMS for diverged applications. Some of the commonly used sensing and actuating principles are introduced in this section.

1.3.1 Sensing Mechanisms

Many microsecond based on different sensing principles for MEMS have been developed [39,40], including chemical sensors, gas sensors, optical sensors, biosensors, thermal sensors, mechanical sensors, etc. Some of the major sensing mechanisms for mechanical microsecond are introduced in the following context.

Piezoresistive Sensing

Piezoresistive sensing uses the resistors varied with the external pressing to measure such physical parameters as pressure, force, accelerometer, flow rate, etc.

A typical structure for piezoresistive microsecond is shown in Figure 1.8, which the resistors are usually built on a silicon diaphragm. The deflection of the diaphragm leads to the dimension change of the resistors, resulting in the resistance changing because of the piezoresistive effect in silicon.

$$\frac{\Delta R}{R} = (1 + 2\nu)\frac{\Delta l}{l} + \frac{\Delta\rho}{\rho} \quad (1.1)$$

where ΔR is the change of the resistance, R is the original resistance, ν is the poisson ratio, Δl is the length change of the resistor, l is the original length of the resistor, $\Delta\rho$ and ρ represent the resistivity change and resistivity of the resistor. It is easily found that the resistance of the resistors used for this type of piezoresistive microsecond is proportional

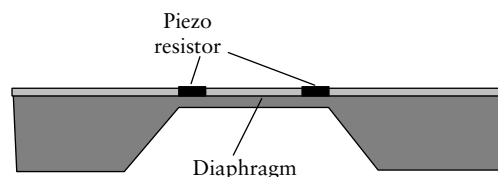


Figure 1.8 A piezoresistive sensing structure

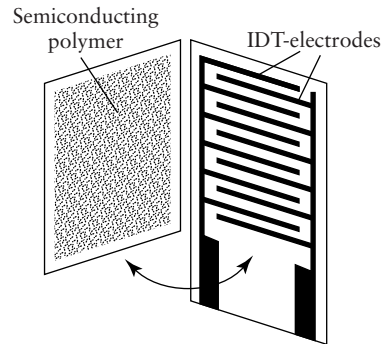


Figure 1.9 Piezoresistive sensing combining IDT and semiconductor polymer [24]

to the external pressure where the resistivity change is ignored, as the dimension change is proportional to the applied pressure.

Another piezoresistive type microsensor is schematically shown in Figure 1.9, in which a semiconductor polymer foil is put on an interdigital transducer's (IDT) electrodes. If a voltage is applied to the electrodes and there is no pressure applied, the resistance is at the level of Mohm. When a force is applied, the resistance decreases because of the current that flows across the shunting polymer foil [41]. Here, the sensing resistance is inversely proportional to the pressure applied.

The performance of the piezoresistive microsecond varies over the temperature and the pressure. The sensitivity of the sensors decreases as temperature increases, and any residual stress generated during the fabrication will also influence the sensitivity of the sensors. The nonlinear deflection of the diaphragm occurs when the high pressure-induced deflection is more than 10 percent of the diaphragm thickness.

Capacitive Sensing

Capacitive sensing uses the diaphragm deformation-induced capacitance change to convert the information of pressure, force, etc., into the electrical signals such as changes of oscillation frequency, time, charge, and voltages. The structure of a typical capacitive microsensor is shown in Figure 1.10, in which an electrode on the flexible diaphragm and the other one on the substrate construct the sensing capacitor. The capacitive microsecond can be used for pressure, force, acceleration, flow rate, displacement, position and pose measurement, etc.

For capacitive microsecond, the capacitance change is not linear with respect to the diaphragm deformation, and also, the small capacitance

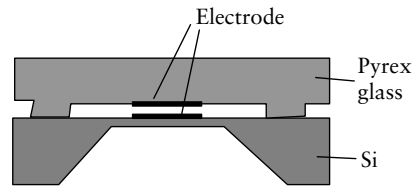


Figure 1.10 Capacitive sensing structure

(generally 1 ~ 3 pF) requires the measurement circuit to be integrated on the chip. But the capacitive sensing was found to have potential for higher performance than piezoresistive sensing in applications requiring high sensitivity, low pressure range, and high stability [40].

Piezoelectric Sensing

Piezoelectric sensing is based on the piezoelectric effect of piezoelectric materials. The electrical charge change is generated when a force is applied across the face of a piezoelectric film. For a piezoelectric disc of a given thickness of t , the voltage (V) generated across the electrode disc (Figure 1.11) when subjected to a stress (T) would be

$$V = gtT \quad (1.2)$$

where g is the piezoelectric voltage coefficient. The piezoelectric sensing is mostly used in the sensors such as pressure sensors, force sensors, velocity and accelerometers, hydrophone, microphone, etc.

Resonant Sensing

Resonant sensing principle is based on the fact that the resonant frequency of a resonator varies with the strain (stress) generated in



Figure 1.11 Piezoelectric sensing

the resonator structure. In the developed resonant microsensors, strain caused by pressure on the diaphragm leads to the natural frequency of a resonator varied. By picking up the natural frequency variation of the resonator, the physical information that caused the strain will be sensed.

For example, the natural resonant frequency of a flexure resonator with both ends fixed can be obtained from [42]

$$f = \frac{4.73^2 b}{2\pi l^2} \left(\frac{E}{12\rho} \right) \left(1 + 0.2366 \left(\frac{l}{b} \right)^2 \varepsilon \right)^{1/2} \quad (1.3)$$

where f is the natural frequency of the fundamental oscillating mode, l the resonator length, b the resonator thickness, E the Young's modulus, ρ the density of the diaphragm material, and ε the strain generated inside the resonator structure. Comparing resonant sensing with piezoresistive sensing, the resonator acts as a kind of strain gauge, the resonant strain gauge that relates the strain with the resonant frequency. Therefore, the gauge factor of this resonant strain gauge can be determined as follows:

$$k_{gf} = \frac{1}{2} \left(\frac{0.2366(l/b)^2}{1 + 0.2366(l/b)^2 \varepsilon} \right)$$

$$\frac{\Delta f}{f} = k_{gf} \varepsilon \quad (1.4)$$

If a strain is 100 ppm, for a 1.2-mm long, 20-micron wide and 5-micron thick resonator strain gauge, the gauge factor can be as high as 3000, while piezoresistive strain gauge factor is only about 2. Because the gauge factor relates directly to the sensitivity of the sensor, the resonant sensing can be used to obtain highly sensitive microseconds. However, resonant sensing usually requires the more complex sensor structure than piezoresistive sensing does; the resonant strain gauges need to be encapsulated from the fluid [43].

IDT (Interdigital Transducers) and SAW (Surface Acoustic Waves) Sensors

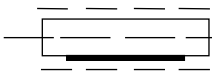
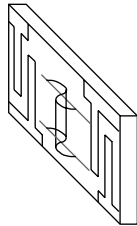
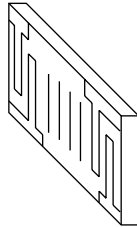
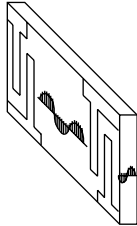
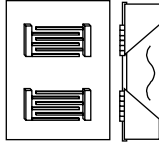
Surface acoustic wave (SAW)-based sensors form an important part of the sensor family, and in recent years these have seen diverse applications ranging from gas and vapor detection to strain measurement [44]. A new breed of SAW-based actuators modeled on MEMS-based microactuators have also been recently announced [44]. IDT and SAW devices were first

used in radar and communication equipment as filters and delay lines, and were recently found to be attractive sensors for various physical variables such as temperature, pressure, force, electric field, magnetic field, and chemical compounds. A SAW device usually is a piezoelectric wafer with interdigital transducers (IDT) and reflectors on its surface. The IDTs provide for the cornerstone of SAW technology. Its function is to convert the electrical energy into mechanical energy, and vice versa, for generating and detecting the SAW. The type of acoustic wave generated in a piezoelectric material depends mainly on the substrate material properties, the crystal cut, and the structure of the electrodes used to transform the electrical energy into mechanical energy. The possibilities of various types of acoustic devices for sensor applications has been explored, and they primarily focus on Rayleigh and shear horizontal surface acoustic wave (SAW and SH-SAW), love wave mode devices, acoustic plate mode (APM), and flexural plate wave (FPW), see Table 1.2.

The Rayleigh wave has both a surface normal component and a surface parallel component that is parallel to the direction of propagation. The Rayleigh wave has two particle displacement components in the sagittal plane. Surface particles move in elliptical paths with a surface normal and a surface parallel component. The electromagnetic field associated with the acoustic wave travels in the same direction. The wave velocity is determined by the substrate material and the crystal cut. The energies of the SAW are confined to a zone close to the surface a few wavelengths thick [44].

A selection of a different crystal cut can yield shear horizontal surface waves instead of Rayleigh waves. The particle displacements of this wave would be transverse to the wave propagation direction and parallel to the plane of the surface. The frequency of operation is determined by the IDT finger spacing and the shear horizontal wave velocity for the particular substrate material. They have shown considerable promise to their application as sensors in liquid media and biosensors [45–47]. In general the SH-SAW is sensitive to mass loading, viscosity, conductivity, and permittivity of adjacent liquid. The configuration of SH-APM devices is similar to the Rayleigh SAW devices, but the wafer is thinner, typically a few acoustic wavelengths. The IDTs generate shear horizontal waves that propagate in the bulk at angles to the surface. These waves reflect between the plate surfaces as they travel in the plate between the IDTs. The frequency of operation is determined by the thickness of the plate and the IDT finger spacing. SH-APM devices are mainly used in liquid sensing and offer the advantage of using the back surface of the plate as the sensing active area.

Table 1.2 Structures of love, SAW, SH-SAW, SH-APM, and FPW devices and comparison of their operation

Device type	Love	Rayleigh SAW	SH-SAW	SH-APM	FPW
Substrate	ST-quartz	ST-quartz	LiTaO ₃	ST-quartz	Si _x N _y /ZnO
Typical frequency	95–130 MHz	80 MHz–1 GHz	90–150 MHz	160 MHz	1–6 MHz
					
U ^a	Transverse	Transverse parallel	Transverse	Transverse	Transverse parallel
U _b	Parallel	Normal	Parallel	Parallel	Normal
Media	Ice to liquid chemosensors	Strain	Gas, liquid	Gas, liquid, chemosensors	Gas, liquid

^a U is the particle displacement relative to wave propagation

^b U_t is the transverse component relative to sensing surface

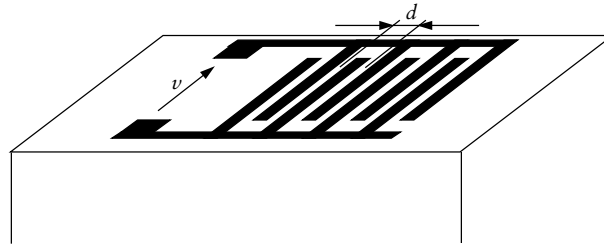


Figure 1.12 Finger spacings and their role in the determination of the acoustic wavelength

Lamb waves, also called *acoustic plate waves*, are elastic waves that propagate in plates of finite thickness and are used for health monitoring of structures and acoustic streaming.

An IDT consists of two metal comb-shaped electrodes placed on a piezoelectric substrate (Figure 1.12). An electric field, created by the voltage applied to the electrodes, induces dynamic strains in the piezoelectric substrate, which in turn launch elastic waves. These waves contain, among others, the Rayleigh waves that run perpendicularly to the electrodes with velocity V_R .

If a harmonic voltage, $v = v_0 \exp(j\omega t)$, is applied to the electrodes, the stress induced by a finger pair travels along the surface of the crystal in both directions. To ensure constructive interference and in phase stress, the distance between two neighboring fingers should be equal to half the elastic wavelength, λ_R .

$$d = \lambda_R/2 \quad (1.5)$$

The associated frequency is known as *synchronous frequency* and is given by

$$f_0 = V_R/\lambda_R \quad (1.6)$$

At this frequency, the transducer efficiency in converting electrical energy to acoustical energy or vice-versa is maximized. The exact calculation of the piezoelectric field driven by the interdigital transducer is rather elaborate [44]. For simplicity, the analysis of the IDT is carried out by means of numerical models. The frequency response of a single IDT can be simplified by the delta-function model [44].

The principle of SAW sensors is based on the fact that SAW traveling time between IDTs changes with the variation of physical variables (Figure 1.13).

One of these IDTs acts as the device input and converts signal voltage variations into mechanical surface acoustic waves. The other

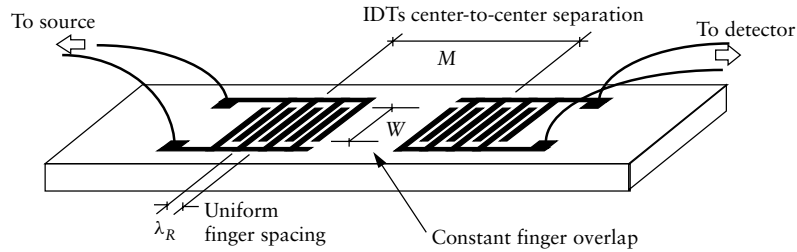


Figure 1.13 Schematic of a SAW device with IDTs metallized onto the surface

IDT is employed as the output receiver to convert the mechanical SAW vibrations back into output voltages. These devices are reciprocal in nature. As a result signal voltages can be applied to either IDT with the same end result.

Acoustic sensors offer a rugged and relatively inexpensive platform for the development of wide-ranging sensing applications. A unique feature of acoustic sensors is their direct response to a number of physical and chemical parameters such as surface mass, stress, strain, liquid density, viscosity, dielectric, and conductivity properties [49]. Furthermore, the anisotropic nature of piezoelectric crystals allows for various angles of cut, and each cut has unique properties. Applications like a SAW-based accelerometer, for example, uses a quartz crystal with an ST-cut, which has an effective zero temperature coefficient [50] and negligible frequency shift through changes in temperature. Again, depending on orientation of crystal cut, various SAW sensors with different acoustic modes may be constructed, with a mode ideally suited toward a particular application. Other attributes include very low internal loss, uniform material density and elastic constants, and advantageous mechanical properties [51]. The principal means of detection of the physical property change involves the transduction mechanism of a SAW acoustic transducer, which involves transfer of signals from the physical (acoustic wave) to the electrical domain [44]. Small perturbations affecting the acoustic wave would manifest as large-scale changes when converted to the electromagnetic (EM) domain because of the difference in velocity between the two waves. Given that the velocity of propagation of the SAW on a piezoelectric substrate is 3488 m/sec and the ac voltage applied to an IDT at a synchronous frequency of 1 GHz. The SAW wavelength is given by $\lambda = v/f = 3488/1 \times 10^9 = 3.488 \times 10^{-6}$ m or 3.488 μm where 1 $\mu\text{m} = 10^{-6}$ m. The EM wavelength in this case is $\lambda c = c/f$ where $c = 3 \times 10^8$ m/sec is the velocity of light. Thus $\lambda c = (3 \times 10^8/1 \times 10^9) = 0.3$ m. The ratio of the wavelengths is $\lambda/\lambda c =$

$3.488 \times 10^{-6}/0.3 = 1.1 \times 10^{-5}$. The sensing action of such transducers involves any influences that will alter the acoustic wave velocity and consequently the associated properties of the wave.

1.3.2 Microactuation

Microactuators are necessary for MEMS to perform physical functions. Many remarkable progresses have been achieved in the development of microactuators [2]. Research and development efforts have been directed toward using different actuation principles and designing various structures for specific applications. A short introduction is given to the microactuation according to its actuation principle.

Electrostatic Actuation

For a simplest parallel plate-type electrostatic microactuator, as shown in Figure 1.14, the electrostatic force is created by applying a voltage across two plates that are separated by insulation layer with certain thickness.

$$F = \frac{\varepsilon \cdot S \cdot V^2}{2d^2} \quad (1.7)$$

where F is the electrostatic force, ε is the dielectric constant of the insulation material, V is the applied voltage, and d is the electrode distance between the two plates.

Electrostatic actuation has been widely used in microactuator developments. The well-known electrostatic microactuators include side-drive silicon micromotor [52], wobble micromotor [53], comb-drive microactuator [54], and out-of-plane diaphragm microactuators [55].

In general, electrostatic actuation is advantageous in the in-chip actuations, in which the high actuation power is not required, and

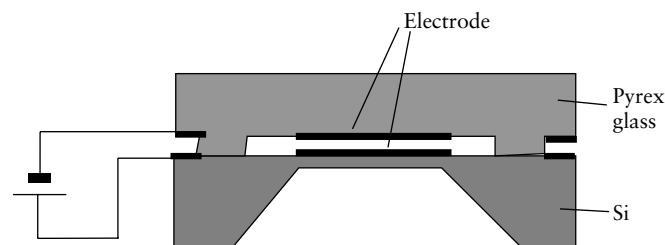


Figure 1.14 Electrostatic actuation

on the other hand, the electrostatic actuators can be easily integrated on a chip from the fabrication point of view, are easily controlled, and consume less input power. Electrostatic microactuators are usually used in the positioning with low power requirements, diaphragm deflection for micropumps, resonators, light modulators, etc. Other actuation principles may be considered when high actuation force or power is required by the applications [2].

Magnetic Actuation

Magnetic microactuation is based on the EM effect, and force is created between the electric coil and magnet. A magnetic microactuator with permanent magnet and planar coil is shown in Figure 1.15 [55], in which the vertical force (along z direction) acting on the magnet (or coil) is calculated from:

$$F = \mu \int \frac{dB}{dz} dV \quad (1.8)$$

where μ is the magnetization of the permanent magnet and is independent of the magnetic induction field \mathbf{B} . One can see that the large volume (dV) of magnet is helpful to obtain large actuating force. This is the reason why LIGA process is preferred in the fabrication of magnetic microactuators [57].

Magnetic actuation is used in the applications requiring high force or torque, but the materials and the processes need to be further developed. How to bond or deposit permanent magnet onto the substrate and fabricate electric coils need to be answered in the future.

Piezoelectric Actuation

Piezoelectric actuation is based on the inverse piezoelectric effect, meaning that when the electric voltage is applied to an asymmetric

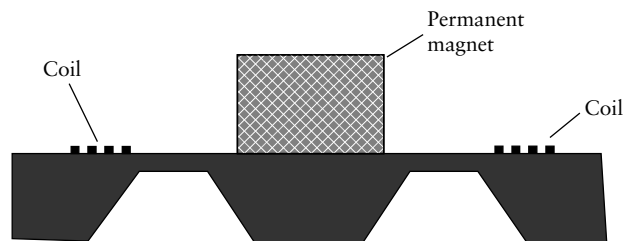


Figure 1.15 Electromagnetic actuation

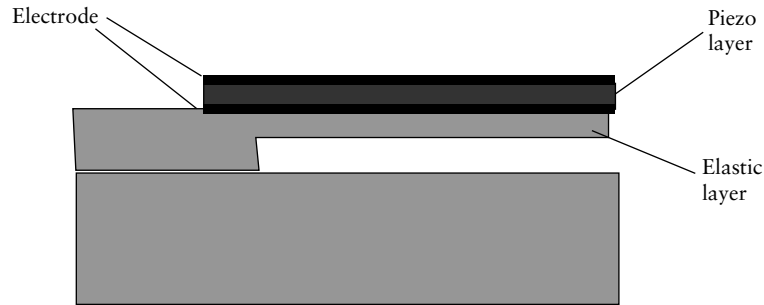


Figure 1.16 Unimorph piezoelectric microactuator

crystal lattice, the material will be deformed in a certain direction. In the conventional piezoelectric actuation, various structures such as cantilever, tube, stacked multilayer structure, Moonie structure, etc. [58] can be considered for different applications. But in microscale, most of the structures used for piezoelectric actuation are based on thin or thick piezoelectric film (bimorph structures). As an example, an unimorph cantilever structure is shown in Figure 1.16. The tip deflection under a voltage of V is provided as follows in the case of one-end-clamped cantilever:

$$\delta(x) = \frac{3t_e(t_e + t_p)E_e E_p x^2 d_{31} V}{E_e^2 t_e^4 + E_e E_p (4t_e^3 t_p + 6t_e^2 t_p^2 + 4t_e t_p^3) + E_p^2 t_p^4} \quad (1.9)$$

where t_e and t_p is the thickness of the elastic and piezo film thickness, E_e and E_p is the Young's modulus of elastic and piezo materials, respectively. The d_{31} is the piezoelectric coefficient, V is the applied voltage. The width and length of elastic and piezo layers are assumed the same [59].

Piezoelectric actuation can be used to supply very high force, but the fabrication processes for piezo materials are to be further developed, and the deposition of thin and thick piezo films on silicon substrate is especially a concern at the moment.

Thermal Actuation

Thermal actuation has been extensively used in microactuators. Thermal actuation is based on a broad spectrum of principles such as mechanical thermal expansion, thermal pneumatic, bimetal effect, shape memory alloy (SMA) effect, etc.

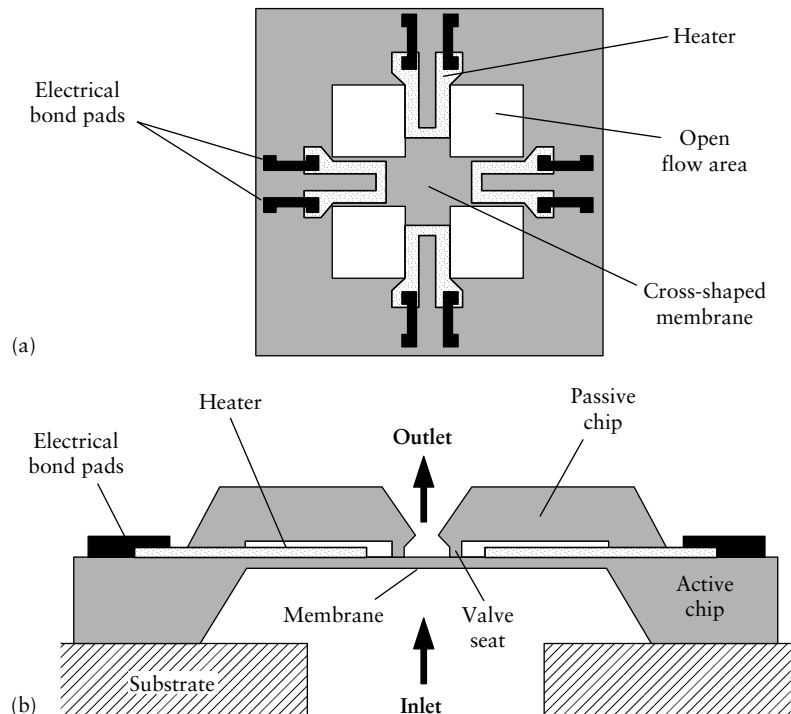


Figure 1.17 Microvalve with thermal actuation [61]

The mechanical thermal expansion leads to the deflection of the beam or diaphragm. A thermally actuated microvalve is shown in Figure 1.17, in which heaters were embedded in the valve diaphragm. When the valve diaphragm is heated, the beam expansion resulted in the upward or downward buckling of the valve diaphragm, controlling *open/off* of the microvalve. High power consumption and the low switching frequency are the concern for the application of this type of microactuators.

Thermal pneumatic actuation uses the thermal expansion of gas or liquid or the phase change between liquid and gas to create the actuation (Figure 1.18). As shown in the Figure, a sealed volume with gas or liquid will expand under the heating, resulting in the diaphragm buckling. This type of microactuators have been widely used in microvalves, micropumps, etc [2]. Large force and displacement are expected from thermal pneumatic actuators, but actuating frequency is very low.

Bimetallic actuation is created when two different materials are layered and heated. In a cantilever bimetallic structure, as shown in Figure 1.19,

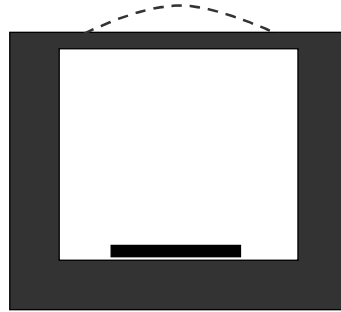


Figure 1.18 Thermal pneumatic actuation

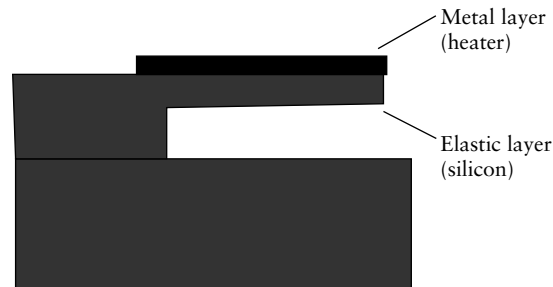


Figure 1.19 Bimetallic actuation (Cantilever)

the end deflection of the cantilever is calculated from as follows:

$$\delta = \frac{3l^2(\alpha_1 - \alpha_2)(t_1 + t_2)\Delta T}{7(t_1 + t_2)^2 - 8t_1t_2 + \frac{4E_1b_1t_1^3}{E_2b_2t_2} + \frac{4E_2b_2t_2^3}{E_1b_1t_1}} \quad (1.10)$$

where l is the length of the cantilever, b_1 , b_2 , t_1 , t_2 , E_1 , E_2 , α_1 , α_2 represent the width and thickness of the two layers, the Young's modulus and thermal expansion coefficient of them, respectively. ΔT is the temperature variation of the structure resulting in the expansion. It is clear that selecting materials with large difference in expansion coefficient is important to obtain large deflection of the actuator.

Bimetallic microactuators can be easily integrated in a silicon micro-machined device and with fairly large force and displacement output. But as other thermal actuation, low actuating frequency limits its application in some cases.

Shape memory alloy (SMA) effect exists in some alloys in which a reversible thermal–mechanical transformation of the atomic structure

of the metal takes place at certain temperatures. At the low temperature, SMA keeps its desired deformed shape at martensitic state. When SMA is heated to a threshold temperature, the deformed martensite is transformed back to austenitic state. SMA wires and thin film are the two structures used in SMA microactuators.

Other Actuations

Other actuations such as electrostrictive actuation, magnetostrictive actuation, electrorheological actuation, chemical actuation, etc., have also been developed for microactuators [2,27]. The selection of actuation for microsystems should be made according to the specific application requirement. More new actuations based on smart materials are expected for MEMS.

1.4 MATERIALS FOR MEMS

A broad spectrum of materials have been incorporated into MEMS. In addition to silicon materials, metal, metal alloy, ceramics, and polymers are the four major material families used for MEMS [2].

1.4.1 Metal and Metal Alloys for MEMS

Thin film metals have been used in IC chips for a long time. Metal-thick film structures are required for some MEMS devices [2]. Microelectroplating and photoforming are used to build thick film metal structures [62,10]. Nickel, copper, and gold have been electroplated to form thick film structures, whereas 3D stainless steel microparts were fabricated by photoforming [10]. Most of the thick film metals are used as structural materials of final devices or as mold inserts for polymer and ceramic micromolding.

Various metal alloys and the related processes have also been developed for MEMS. CoNiMn thin films were used as permanent magnet materials for magnetic actuation. NiFe perm alloy thick films were electroplated on silicon substrate for magnetic microelectromechanical systems devices, such as micromotors, microactuators, microsecond, and integrated power converters, which envisages new micropower magnetics on a chip with integrated circuits [63]. TiNi shape memory alloy films were sputtered on substrate for SMA sensing and actuating [64]. TbFe and SmFe thin films were used for magnetostrictive actuation [65].

1.4.2 Polymer for MEMS

Polymer has been extensively used as both structural and functional materials for microdevices.

As structural materials, elasticity, optical property, and biocompatibility of polymers are used in most microdevices. Various polymer devices are made from thin polymer films, thick polymer films, and 3D polymer microstructures. Some of the polymers and the related processes for polymer structures fabrication are listed in Table 1.3.

It should be pointed out here that the structural polymers mentioned earlier can also be used to construct sensing and actuating components for MEMS, just like silicon and polymer can be used to build microsecond and actuators, although they act as structural materials too. Polymer strain gauges and capacitors can serve as sensing element for piezoresistive and capacitive microsecond [19]. Electrostatic polymer microactuators have been developed from polyimide bellow structures [71]. Another important point is that the wafer polymer microfabrication process is being developed for polymer microdevices, and the batch fabrication of polymer MEMS is not of concern any more.

Because the limited sensing and actuating mechanisms can be used to develop polymer MEMS just from structural polymers, a large species

Table 1.3 Polymers and fabrication processes for MEMS

Polymer name	Structure	Process	Property utilized and reference
Polyimide	Thin film	Coating	Elasticity [34]
Silicon rubber	Thick film	Molding	Elasticity [66]
Parylene C	Thin film	Coating	Vapor barrier [66]
PMMA	Thick film	LIGA, hot-embossing	Elasticity, optical property [5,67]
Polycarbonate	Thick film	Hot embossing	Elasticity, optical transparency [68]
Polydimethyl siloxane (PDMS)	Thick film	Molding	Elasticity, biomedical compatibility [69]
Epoxy resin	Thick film	Molding	Encapsulation, resistance to large PH range [69]
Polyester	Thick film	Casting	Elasticity [70]
Polysulfone	Thick film	Molding	[19]
Acrylate, urethane, epoxy, etc.	3D	Microstereo-lithography	[8,9,17,18,23]

Table 1.4 Functional polymers for MEMS

	Functional property	Applications
PVDF	Piezoelectricity	Sensor/actuator
Poly(pyrrole)	Conductivity	Sensor/actuator/ electric connection
Fluorosilicone	Electrostrictivity	Actuator [72]
Silicone	Electrostrictivity	Actuator [72]
Polyurethane	Electrostrictivity	Actuator [72]

of functional polymers have been developed for MEMS during the past several years [20]. Some of the functional polymers used for MEMS are listed in Table 1.4.

Functional polymer solid powder composites with magnetic and magnetostrictive properties have been developed for function polymer microdevices. The polymer-bonded Terfenol D composites showed excellent magnetostrictivity that can be used for microactuation [73]. The polyimide-based ferrite magnetic composites were used as polymer magnets for magnetic microactuators [74].

In addition to being used as sensing and actuating materials, polymer has also been used for electronic materials. Polymer transistors have been developed [75]. Therefore, integrating polymer sensors, actuators, and electronics into polymer MEMS will be practical for some special applications.

1.4.3 Other Materials for MEMS

Ceramics are another major species of materials used for MEMS. In fact, SiO_2 and Si_3N_4 thin films have ever been used for semiconductor devices and silicon MEMS devices. The thick ceramic film and 3D ceramic structures are also necessary for MEMS for special applications. For example, ceramic pressure microsecond sensors have been developed for pressure measurement at the high-temperature environment [76], silicon carbide MEMS for harsh environments [21], etc. In addition to these structural ceramics, some function ceramics such as ZnO, PZT, etc., have also been incorporated into MEMS. The fabrication processes developed for ceramic MEMS include screen printing, tape lamination, micromolding, sol-gel, microstereolithography, etc.

Other materials such as diamond, GaAs, lubrication materials such as fluorocarbon, SAM, DLC (diamond-like carbon), etc., quartz, and so forth are also broadly used in MEMS for their special characteristics [2].

1.5 SMART ELECTRONICS AND CONFORMAL ANTENNAS

The development of integrated smart electronics involves microelectronics circuitry, low-power signal-processing electronics, microcontroller, and wireless communication between microseconds and microactuators. Three different approaches are pursued with silicon devices:

- 1 CMOS (complementary metal oxide silicon) microelectronics first followed by MEMS device integration using polysilicon surface micromachining [77]
- 2 Micromechanics-first followed by CMOS integration [77] (Figure 1.20 and 1.21) and
- 3 Flip-chip integration of MEMS chips with that of microelectronics circuitry chips [78] (Figure 1.22).

The flip-chip integration is very attractive for both silicon and polymeric MEMS devices. The electronics are fabricated on silicon substrates; the MEMS may be fabricated either on silicon or on polymeric substrates. Then the electronics and the MEMS are connected using solder bumping.

A built-in electronics system called *BIFET process* has been conceived in Delft University of Technology [79]. A simplified version of it with surface acoustic wave devices is shown in Figure 1.23 [80].

Polyimide coating of 1–2 mm may also be used for compatibility with the smart skin. For local intelligence and decision making, one could add ASIC to the electronics. An ASIC is a semiconductor device designed for a specific application. The two major categories of ASIC technology are array-based and cell-based. Array-based ASICs configure a specific design at metal layers, whereas cell-based ASICs are uniquely fabricated at all layers of the silicon process including the diffusion layers. The chip has a wide range of applications. In conjunction with sensors such as accelerometers, it can be used to design smart sensors. The chip can play a vital role in engine controllers and in pressure measurements using vibrating-type transducers.

For polymeric-based MEMS, the electronics is usually done in silicon, and the processes such as photoforming and AMANDA are employed to achieve the desired devices. With the invention of organic thin film transistor, it now seems possible to fabricate polymeric MEMS devices with built-in electronics.

The incorporation of IDT and SAW-based wireless architecture is, however, ideal for polymeric devices, as there is no electronics necessary at the sensor location.

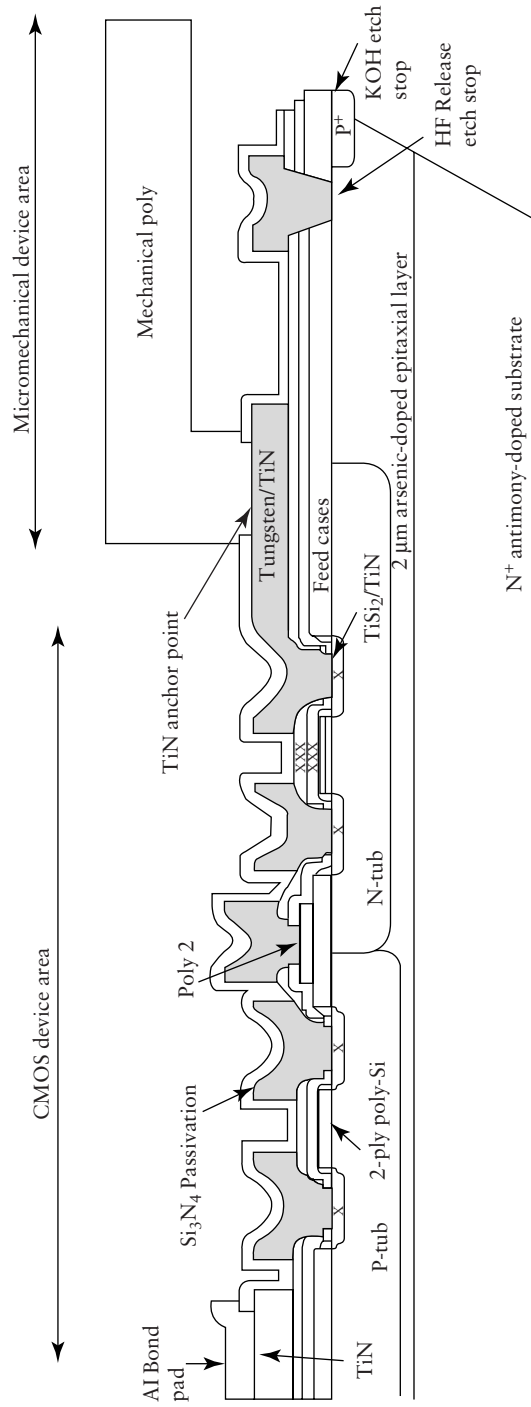


Figure 1.20 CMOS first, micromechanics second [91]

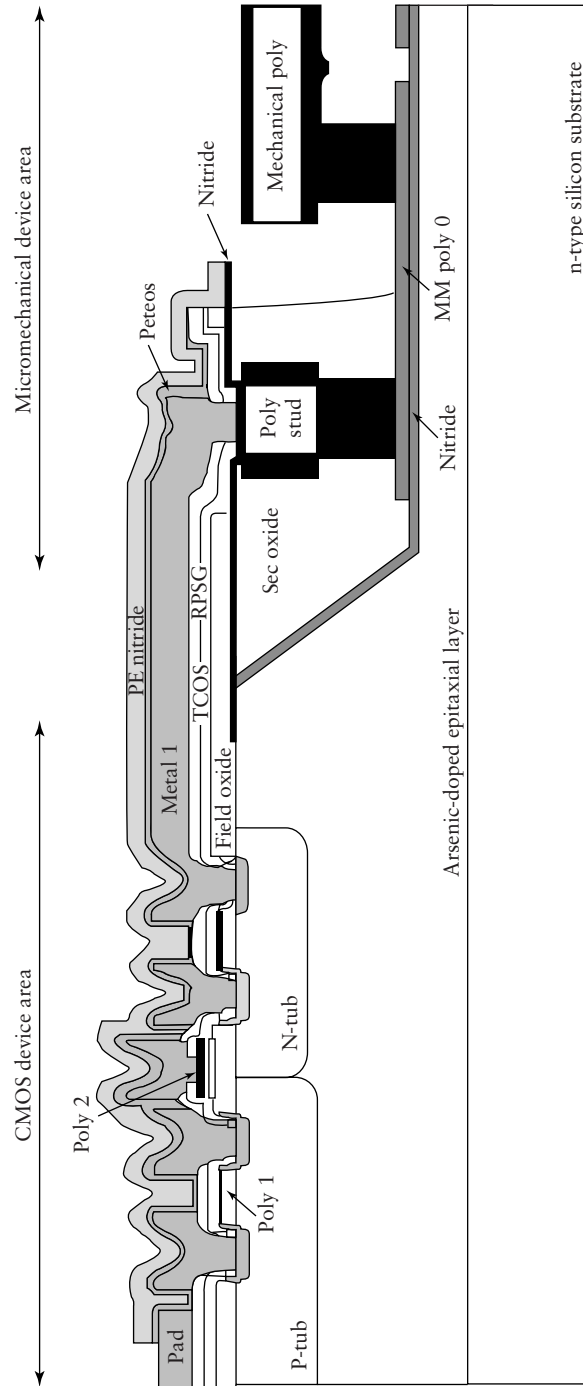


Figure 1.21 Micromechanics first, CMOS second [91]

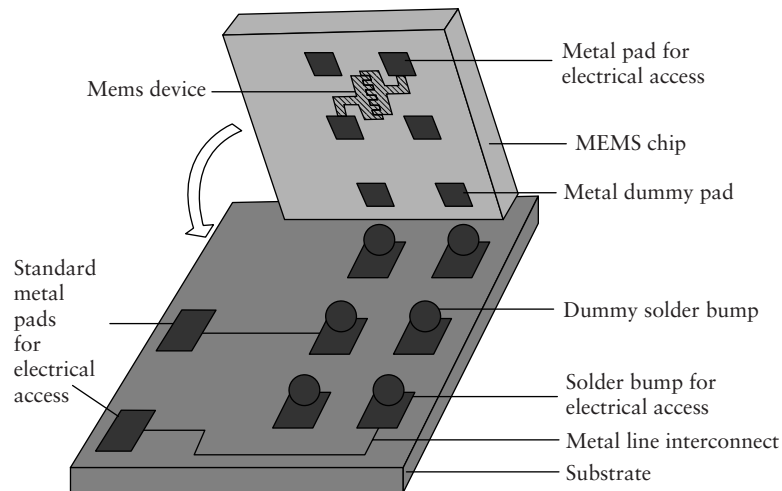


Figure 1.22 Flip-chip bonding [92]

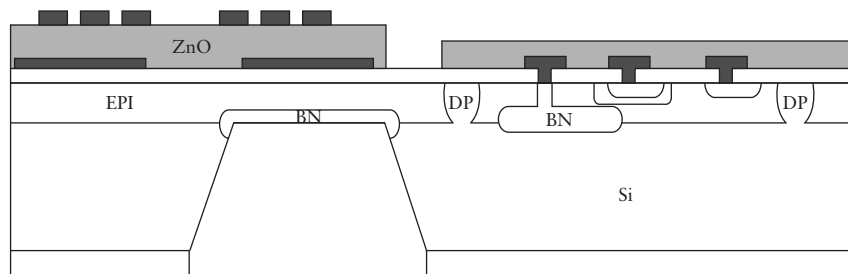


Figure 1.23 Delft field transistor [93]

To obtain a high sensitivity, spacing sensors are usually constructed as electric oscillators using the SAW device as frequency control components. By accurately measuring the oscillation frequency, a small change of the physical variables can be detected by the sensors. A typical SAW oscillator sensor schematic is shown in Figure 1.24. An amplifier connects two IDTs on a piezoelectric wafer so that oscillations result because of the feedback of the SAW propagating from one IDT to the other. The oscillation frequency satisfies the condition that the total phase shift of the loop equals $2n\pi$ and varies with the SAW velocity or the distance between the IDTs. The oscillator includes an amplifier and requires electrical power supply and cannot be wireless. The operating frequency range of the SAW devices is from 10 megahertz to a few gigahertz that directly matches the frequency range of radios

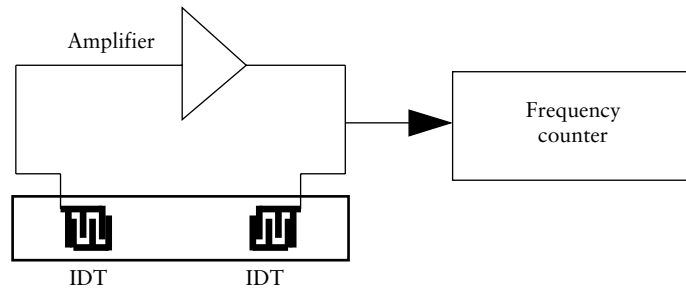


Figure 1.24 Schematic diagram of an oscillator SAW sensor with a SAW resonator

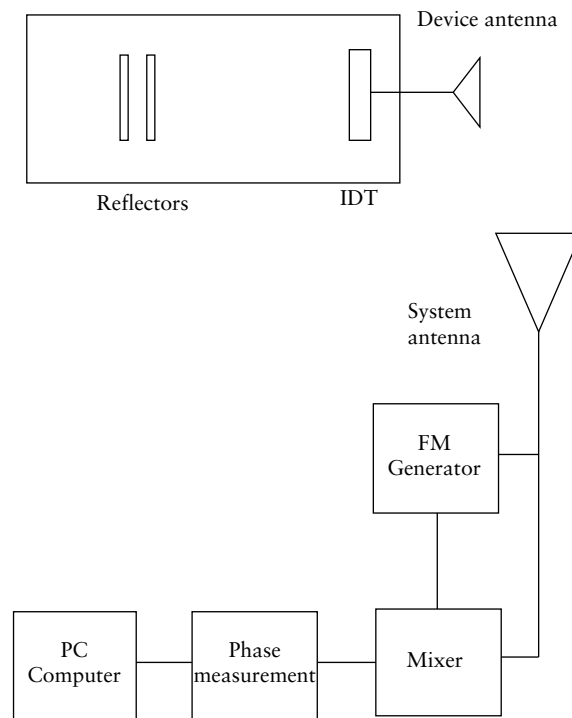


Figure 1.25 Schematic diagram of remote reading sensor system with passive SAW sensor

and radar. When an IDT is directly connected to an antenna, SAW can be excited remotely by electromagnetic waves. The fact suggests that it is possible to realize passive, wireless, or remotely operable SAW devices. The application to remote sensors was first reported in [81]. The temperature of a passive SAW device with a small antenna was remotely read out by a microwave system [82]. The schematic diagram of IDT

and reflectors in Figure 1.25 shows the basic operating principle of the system for a wireless communication. An IDT and two reflectors are made on the surface of a piezoelectric crystal wafer. These micro-IDT and SAW sensors can be fabricated using microlithographic process.

The IDT connects directly to a small antenna called the *device antenna*. This antenna-IDT configuration is able to convert the microwave signal from air to SAW signal on the wafer surface and vice versa. The reading system has a linear frequency modulated (FM) signal generator. The FM signals are transmitted by a system antenna. The signals are received by the device antenna and converted by the antenna-IDT to SAWs propagating along the surface of the wafer. The echoes from the two reflectors are picked up by the antenna-IDT and sent back to system antenna. The echo signals are delayed copies of the transmitted FM signal. The delay times mainly depend on the velocity of the SAWs and distance between the IDT and the reflectors. A mixer that takes the transmitted FM as reference signal outputs the signals of frequency difference between the echoes and the transmitted signals. Because the transmitted signal is linear frequency modulated, the frequency difference is proportional to the delay time. By using spectrum analysis technique like FFT (fast fourier transform), the two echo signals can be separated in the frequency domain, as the delay times are different.

1.6 WIRELESS TELEMETRY SYSTEMS

Wireless remote and continuous telemetry systems for application to smart structures can be achieved using Penn State's novel antenna architecture using ferroelectric on-line or filter phase shifters to interact with MEMS, piezoelectric polymer skins, and SAW sensors, wherein the communication from sensors to control systems and back to the actuators is accomplished by wireless telemetry using antennas specially designed for such purpose and integrated into the structure.

The ferroelectric ceramics are used to develop new, lightweight, flat, and large bandwidth antennas whose output beams can be steered electronically (beam steering) by tuning the dielectric properties of the ceramic. The two plane electronics scanning of the phased array depends largely on phase shifters. The use of printed microstrip or fractal antenna as radiating element in phased array leads to significant reduction of size, weight, and production cost. Integration of the feeding network with the phase shifters in the same substrate plane form a light, compact, and flat antenna system particularly for air borne applications.

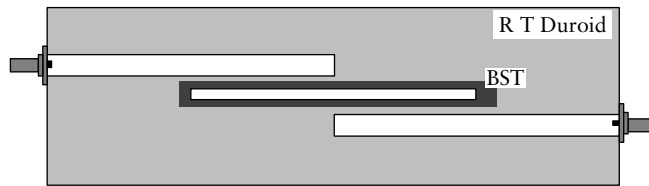


Figure 1.26 Schematic diagram of the filter phase shifter

In [83], it has been shown that a filter phase shifter is an ideal one for many types of electronically steerable antenna (Figure 1.26).

The configuration is easily adaptable with the microelectronics processing. The ferroelectric films can be deposited on the substrate on which the feed line conductors can be screen printed, and an electronically steerable antenna may thus be conceived for beam steering (see Figure 1.27). Beam steering (see Figure 1.28) can be used to advantage for monitoring and communicating with several sensors and actuators distributed over a large structure using a single central antenna.

A sensor bus can be used when sensing many parameters at the same time. The sensors can be electronically scanned, and the information is passed on to the microcontroller. Separate software code has to be

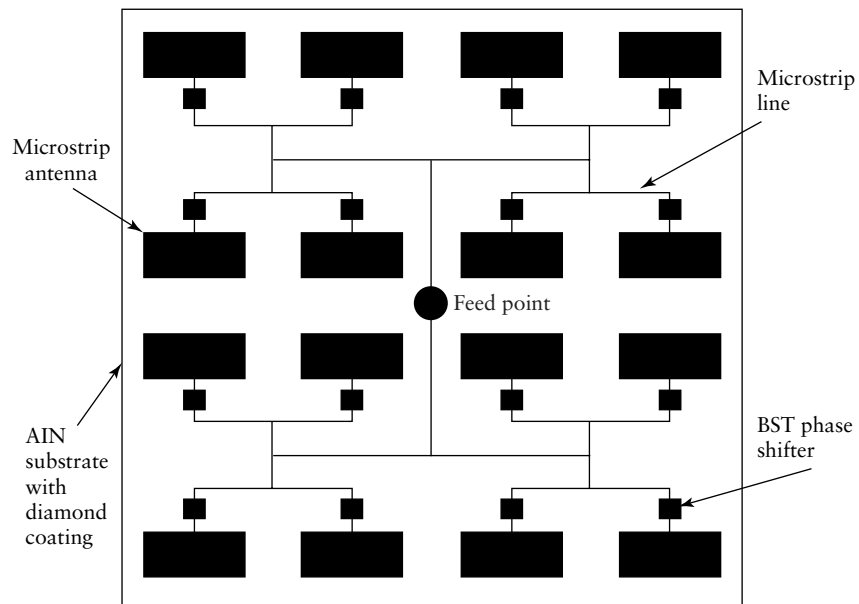


Figure 1.27 Microstrip antenna with ferroelectric phase shifters

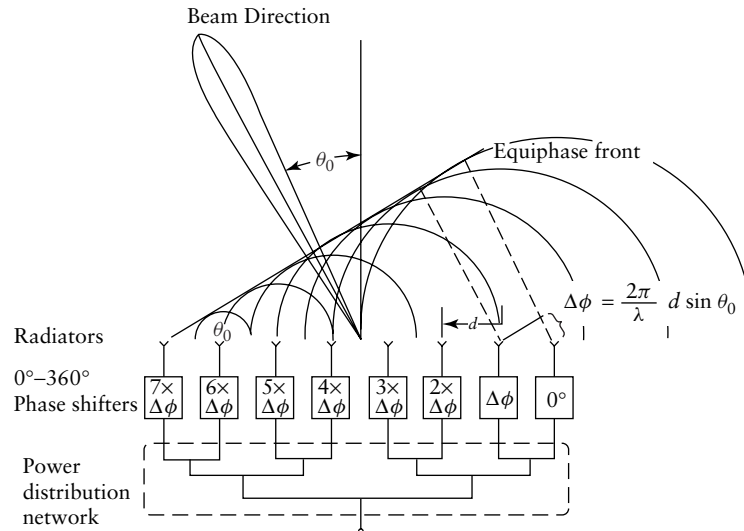


Figure 1.28 Concept of beam steering

assigned in the microcontroller to each sensor. The wireless communication link consists of a transmitter and receiver with a message format consisting of eight data bits preceded by a starter bit and followed by parity bit and stop bit. The antenna for this application is a conformal one employing high dielectric and low-loss ferroelectric material with tunable capability. Planar phase shifters controlled only by bias voltage are used for electronic steerability [84–89].

For field implementation of a remote sensor reader system, a self-contained, portable system has been developed by HVS Technologies. Figure 1.29 shows the layout of such a system.

This system operates in the 905–925 MHz range. The circuit operation is as follows: The signal is pulse FM modulated. A pulser would synchronize the DC voltage ramp circuit, voltage controlled oscillator (VCO) output, and the A/D converter during pulses 16-ms long. During the pulse, the DC voltage ramp circuit would linearly tune the VCO from 905 to 925 MHz. The VCO output is controlled by a diode switch, then amplified to 50 mW by a high isolation amplifier. A coupler diverts a sample of the signal to the LO (local oscillator) input of the mixer. A circulator sends the transmit signal to the antenna and sends the reflected signal through an automatic gain control amplifier to the RF input of the mixer. A low-pass filter removes any noise and high-frequency signals. Then the signal is digitized at 10 Msps and 10-bit resolution. A programmable DSP (digital signal processing) chip such as the TI

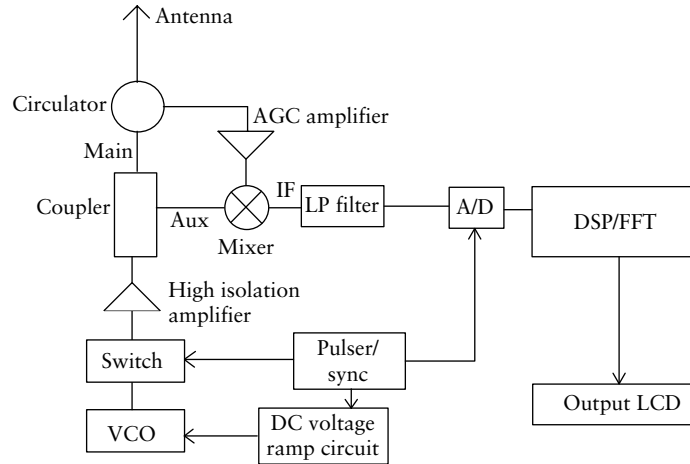


Figure 1.29 System for remote sensing application

TMS320C3X is used to extract delayed information and compute the desired parameter. This is then output to a LCD.

1.7 SCOPE OF THIS BOOK

During the past seven to eight years, novel microfabrications capable of fabricating 3D microstructures with various materials have been developed for MEMS. In this book, some free-form 3D-microfabrication processes, AMANDA process, smart materials incorporation into MEMS, etc., are introduced with the aspect of principles, fabrication prototypes, possible applications of the processes and the devices, etc. Besides, the novel organic thin film transistor (TFT) technology is also introduced to explore the possibility to integrate TFT into MEMS.

In Chapter 2, fundamentals on polymerization, radiation curing, especially the UV radiation and the applications of UV radiation are presented as many novel 3D-microfabrication processes are still based on UV radiation-curing principles.

Principles of stereolithography are introduced in Chapter 3. In detail, photochemical theory for SL, SL system setup, and general microstereolithography are presented.

Two different microstereolithography (MSL) techniques – scanning MSL and projection MSL – are introduced in Chapter 4 and 5, respectively. In addition to the process principles, several photographs of the fabrication samples are shown for better understanding the uniqueness of the processes.

Ceramic MSL, metal–polymer MSL, spatial forming, and localized electrochemical deposition processes are introduced in Chapter 6 for the incorporation of different materials into 3D-MEMS devices.

Combined silicon and polymer structures are demonstrated as important for many MEMS applications, photoforming, MSL integrated with thick film lithography, and AMANDA processes developed for this purpose and are introduced in Chapter 7.

Micromolding as a mass microfabrication approach is introduced in Chapter 8.

Some MEMS devices fabricated by the earlier-mentioned microfabrication processes are presented in Chapter 9 as applications. Organic thin film transistor technology is introduced in Chapter 9 as an example of polymer for electronic devices and MEMS, in which the organic semiconductor materials and development of devices is presented.

REFERENCES

1. Fujita, H, (1996). ‘Future of actuators and microsystems,’ *Sensors and Actuators*, **A56**, 105–111.
2. Fujita, H, (1998). ‘Microactuators and micromachines,’ *Proc. IEEE*, **86**, (8), 1721–1732.
3. Kovacs, G T A, Maluf, N I, Petersen, K E, (1998). ‘Bulk micromachining of silicon,’ *Proc. IEEE*, **86**, (8), 1536–1551.
4. Bustillo, J M, Howe, R T and Muller, R S, (1998). ‘Surface micromachining for microelectromechanical systems,’ *Proc. IEEE*, **86**, (8), 1552–1574.
5. Guckel, H, (1998). ‘High-aspect-ratio micromachining via deep X-ray lithography,’ *Proc. IEEE*, **86**, (8), 1586–1593.
6. Xia, Y and Whitesides, G M, (1998). ‘Soft lithography,’ *Angew. Chem., Int. Ed.*, **37**, 550–575.
7. Varadan, V K and Varadan, V V, (1996). ‘Three dimensional polymeric and ceramic MEMS and their applications,’ *Proc. SPIE*, **2722**, 156–164.
8. Ikuta, K and Hirowatari, K, (1993). ‘Real three dimensional microfabrication using stereo lithography and metal molding,’ *Proc. IEEE MEMS*, 42–47.
9. Katagi, T and Nakajima, N, (1993). ‘Photoforming applied to fine machining,’ *Proc. IEEE MEMS*, 173–178.
10. Taylor, C S, et al., (1994). ‘A spatial forming – a three dimensional printing process,’ *Proc. IEEE MEMS*, 203–208.
11. Thornell, G and Johansson, S, (1998). ‘Microprocessing at the fingertips,’ *J. Micromech. Microeng.*, **8**, 251–262.
12. Middelhoek, S and Audet, S A, (1989). *Silicon Sensors*, Academic Press, London.

13. Peterson, K E, 'Silicon as a mechanical material,' *Proc. IEEE*, 70 (1982) 420–457.
14. Bryzek, J, Peterson, K and McCulley, W, (1994). 'Micromachines on the march,' *IEEE Spectrum*, May, 1994, 20–31.
15. Fan, L -S, Tai, Y -C and Muller, R S, (1987). 'Pin joints, gears, springs, cranks and other novel micromechanical structures,' *Proc. Transducers*, 849–852.
16. *Proc. IEEE MEMS*, 1993–1997.
17. Varadan, V K, (ed.), (1995). 'Smart Electronics,' vol. 2448, *Proc. SPIE*, Bellingham, WA.
18. Tani, J and Esashi, M, (eds.), (1995). 'Intelligent Materials and Robots,' *Proceedings of the International Symposium on Microsystems*, Tohoku University, Japan.
19. Varadan, V K and Varadan, V V, (1995). '3D MEMS Structures and their Applications' Invited Paper presented at the International Symposium on Microsystems, Intelligent Materials, and Robots, Tohoku University, Japan.
20. Carraway, D L, (1991). 'The use of silicon microsecond in smart skins for aerodynamic research' *International Congress on Instrumentation in Aerospace Simulation Facilities*, 413–422.
21. Chin, L C, Varadan, V V and Varadan, V K, (1994). 'Hybrid Finite Element Formulation for Periodic Piezoelectric Arrays Subjected to Fluid Loading,' *Int. J. Numer. Methods Eng.*, 37, 2987–3003.
22. Aeidel, H, (1987). 'The mechanism of anisotropic silicon etching and its relevance for micromachining,' *Proceedings of the international conference on Solid-State Sensors and Actuators*, Tokyo, Japan, 120–125.
23. Shaw, K W, Zhang, Z L and MacDonald, N C, (1994). 'SCREAM: a single mask, single-crystal silicon, reactive ion etching process for microelectromechanical structures,' *Sensors and Actuators A*, 40, 63–70.
24. Fatikow, S and Rembold, U, (1997). *Microsystems Technology and Microrobotics*, Springer, New York.
25. Schmidt, M A, (1998). 'Wafer-to-wafer bonding for microstructure formation,' *Proc. IEEE*, 86 (8), 1575–1585.
26. Ko, W H, Suminto, J T and Yeh, G J, (1985). 'Bonding techniques for microsecond,' *Studies in Electrical and Electronic Engineering*, 20, 41–61.
27. Madou, M, (1997). 'Fundamentals of microfabrication,' CRC Press, Boca Raton, Fla.
28. Rogner, A, et al., (1991). 'LIGA-based flexible microstructures for fiber-chip coupling,' *J. Micromech. Microeng.*, 1 (3), 167–170.
29. Cohen, A, et al., (1999). 'EFAB: rapid, low-cost desktop micromachining of high aspect ratio true 3D MEMS,' *Proc. IEEE MEMS*, 244–251.
30. Madden, J D and Hunter, I W, (1996). 'Three-dimensional microfabrication by localized electrochemical deposition,' *J. Microelectromech. Syst.*, 5 (1), 24–32.

31. Bertsch, A, Lorenz, H and Renaud, P, (1998). 'Combining microstereolithography and thick resist UV lithography for 3D microfabrication,' *Proc. IEEE MEMS*, 18–23.
32. Takagi, T and Nakajima, N, (1994). 'Architecture combination by micro photoforming process,' *Proc. IEEE MEMS*, 211–216.
33. Schomburg, W K, et al., (1998). 'AMANDA – low-cost production of microfluidic devices,' *Sensors and Actuators*, A 70, 153–158.
34. Ruprecht, R, Hanemann, T, Piottter, V, Hau elt, J, (1998). 'Polymer materials for microsystem technologies,' *Microsystem Technologies*, 5 44–48.
35. Mehregany, M, Zorman, C A, Rajan, N and Wu, C H, (1998). 'Silicon carbide MEMS for harsh environments,' *Proc. IEEE*, 86, 1594–1610.
36. Ayerdi, I, Castano, E, A. Garcia-Alonso and Gracia, J, (1997). 'High-temperature ceramic pressure sensor,' *Sensors and actuators*, A60, 72–75.
37. Zhang, X, Jiang, X N and Sun, C, (199). 'Micro-stereolithography of polymeric and ceramic microstructures,' *Sensors and Actuators*, A77 (2), 149–156.
38. Jiang, X N, Sun, C and Zhang, X, 'Microstereolithography of 3D complex ceramic microstructures and PZT thick films on Si substrate,' *ASME MEMS*, 1, 67–73.
39. Fatikow, S and Rembold, U, (1997). *Microsystem technology and micro-robots*, Springer Publishing New York.
40. Rai-choudhury, P, (1997). *Handbook of microlithography, micromachining and microfabrication*, SPIE Optical Engineering Press.
41. Witte, M and Gu, H, 'Force and position sensing resistors: an emerging technology,' *Proceedings of the international conference on new actuators*, Bremen, Germany, 168–170.
42. Ikeda, K, et al., (1990) 'Silicon pressure sensor integrates resonant strain gauge on diaphragm,' *Sensors and Actuators*, A21–23, 146–150.
43. Harada, K, Ikeda, K, Kuwayama, H and Murayama, H, (1999). 'Various applications of resonant pressure sensor chip based on 3-D micro-machining,' *Sensors and Actuators*, A73, 261–266.
44. Campbell, C, (1998). 'Surface Acoustic Wave Devices and their Signal Processing Applications,' Academic Press, London, UK.
45. Nakamura, N, Kazumi, M and Shimizu, H, (1977). 'SH-type and Rayleigh type surface waves on rotated Y-cut LiTaO₃,' *Proceedings of IEEE Ultrasonics Symposium*, 819–822.
46. Shiokawa, S and Moriizumi, T, (1987). 'Design of SAW sensor in Liquid,' *Proceedings of 8th Symposium on Ultrasonic Electronics*, Tokyo.
47. Kondoh, J, Matsui, Y and Shiokawa, S, (1993). 'New biosensor using shear horizontal surface acoustic wave device,' *Jpn. J. Appl. phys.*, 32, 2376–2379.
48. Varadan, V K and Varadan, V V, (1997), 'Microsensors, actuators, MEMS, and electronics for smart structures,' Rai-Choudhury P (ed.) *Handbook of Microlithography, Micromachining, and Microfabrication*, Vol. 2: Micro-machining and Microfabrication, SPIE Optical Engineering Press, 617–688.

49. Grate, J W, Martin S J and White, R M, (1993) 'Acoustic wave microseconds'. *Part 1, Analytical Chemistry*, **65**, 940–948.
50. Varadan V K and Varadan, V V, (1996). 'IDT, SAW and MEMS Sensors for measuring deflection, acceleration and ice detection of aircraft,' *SPIE*, **3046**, 209–219.
51. Grate, J W, Martin S J and White, R M, (1993). 'Acoustic Wave Microsensors'. *Part 1I, Analytical Chemistry*, **65**, 987–996.
52. Fan, L -S, Tai, Y -C and Muller, R S, (1989). 'IC-processed electrostatic micromotors,' *Sensors and Actuators*, **20**, 41–48.
53. Mehregany, M, Nagarkar, P, Sentura, S D and Lang, J H, (1990). 'Operation of microfabricated harmonic and ordinary side-drive motors,' *Proc. IEEE MEMS*, 1–8.
54. Tang, W C, Nguyen, T C H and Howe, R T, (1989). 'Laterally driven polysilicon resonant microstructures,' *Sensors and Actuators*, **20**, 25–32.
55. Zengerle, R, Ritcher, A and Sandmaier, H, (1992). 'A micro membrane pump with electrostatic actuation,' *Proc. IEEE MEMS*, 9–24.
56. Benecke, W, (1991). 'Silicon-microactuators: Activation mechanisms and scaling problems,' *Transducers*, 46–50.
57. Guckel, H, (1998). 'Progress in Magnetic microactuators,' *Microsys. Technol.*, **5**, 59–61.
58. Uchino, K, (1997). 'Piezoelectric actuators and ultrasonic motors,' *Kluwer Academic Publishers*, Norwell, MA.
59. Devoe, D L and Pisano, A, (1997). 'Modeling and optimal design of piezoelectric cantilever microactuators,' *J. Microelectromech. Syst.*, **6** (3), 266–270.
60. Timeshenko, S P, (1925). 'Analysis of bi-metal thermostats,' *J. Optical Soc. Amer.*, **11**, 233–255.
61. Lisec, T, et al., (1994). 'Thermally driven microvalve with buckling behavior for pneumatic applications,' *IEEE MEMS*, 13–17.
62. Romankiw, L T, (1997). 'A path: from electroplating through lithographic masks in electronics to LIGA in MEMS,' *Electrochimica Acta*, **42** (20–22), 2985–3005.
63. Ahn, C H and Allen, M G, (1998). 'Micromachined planar inductors on silicon wafers for MEMS applications,' *IEEE Transactions on Industrial Electronics*, **45** (6), 866–876.
64. Ohta, A, Bhansali, S, Kishimoto, I and Umeda, A, (1998). 'Development of TiNi shape memory alloy film deposited by sputtering from separate Ti and Ni targets,' *Proc. of SPIE*, **3512**, 138–145.
65. Honda, T, Arai, K I and Yamaguchi, M, (1997). 'Basic properties of magnetostrictive actuators using Tb-Fe and Sm-Fe thin films,' *IEICE Transactions on Electronics*, **E80-C** (2), 232–238.
66. Grosjean, C, Yang, X and Tai, Y C, (1999). 'A practical thermopneumatic valve,' *Proc. IEEE MEMS*, 147–152.
67. Becker, H and Heim, U, (1999). 'Silicon as tool material for polymer hot embossing,' *Proc. IEEE MEMS*, 228–231.

68. Pan, L W, Lin, L W and Ni, J, (1999). 'Cylindrical plastic lens array fabricated by a micro intrusion process,' *Proc. IEEE MEMS*, 217–221.
69. Armani, D, Liu, C and Aluru, N, (1999). 'Re-configurable fluid circuits by PDMS elastomer micromachining,' *Proc. IEEE MEMS*, 222–227.
70. Bohm, S, Olthuis, W and Bergveld, P, (1999). 'A plastic micropump constructed with conventional techniques and materials,' *Sensors and Actuators*, 77, 223–228.
71. Minami, K, Morishita, H and Esashi, M, (1999). 'A bellows-shape electrostatic microactuator,' *Sensors and Actuators*, 72, 269–276.
72. Pelrine, R, Kornbluh, R, Joseph, J and Chiba, S, (1997). 'Electrostriction of polymer films for microactuators,' *Proc. IEEE MEMS*, 238–243.
73. Ruiz de Angulo, L, Abell, J S and Harris, I R, (1996). 'Magnetostrictive properties of polymer bonded Terfenol-D,' *Journal of Magnetism and Magnetic Materials*, 157–158, 508–509.
74. Lagorce L K and Allen, M G, (1996). 'Micromachined Polymer Magnets,' *ISAF*, 85–90.
75. *Organic thin film transistors*, (1999).
76. Jennifer, M and Allen, M G, (1999) 'Wireless micromachined ceramic pressure sensors English,' *Proc. IEEE MEMS*, 511–516.
77. Smith, J H, Montage, S and Sniegowski, J J, 'Material and processing issues for the monolithic integration of microelectronics with surface-micromachined polysilicon sensors and actuators,' Karen W. Markus, (ed.), *Micromachining and Microfabrication Process Technology*, Vol. 2639, 1995.
78. Markus, K W, et al., (1995). 'MEMS infrastructure: The Multi-User MEMS Processes (MUMPS),' Karen W. Markus (ed.) *Micromachining and Microfabrication Process Technology*, Vol. 2639, SPIE.
79. Nanver, L K, Goudena, E J G and van Zeijt, H W, (1993). 'DIMES-01, a baseline BIFET process for smart sensor experimentation,' *Sensors and Actuators A*, 36, 136–147.
80. Vellekoop, M J, Lubking, G W, Sarro P M and Venema, A, (1994). 'Integrated-circuit-compatible design and technology of acoustic-wave-based microsecond,' *Sensors and Actuators A*, 44, 249–263.
81. Bao, X Q, Varadan, V V and Varadan, V K, (1987). 'SAW temperature sensor and remote reading system,' *Proc. IEEE Ultrasonic Symposium*, 1, 583–585.
82. Varadan, V K, Varadan, V V and Bao, X Q, 'Wireless Telemetry Systems and their Applications,' *Journal of Smart Materials and Structures*, accepted for publications.
83. Varadan, V K, et al., (1994). 'A novel microwave planar phase shifter,' *Microwave Journal*, 38, 244–254.
84. Varadan, V K, et al., (1992). 'Ceramic Phase Shifters for Electronically Steerable Antenna Systems,' *Microwave Journal*, 35, 116.
85. Varadan, V K, et al., (1994). 'A novel microwave planar phase shifter,' *Microwave Journal*, 38 (4), 244–254.

86. Jose, K A, et al., (1993). 'Experimental Investigations of Electronic Beam Steering Array Antennas,' *Journal of Wave-Materials Interaction*, **8**, 311.
87. Varadan, V K, Varadan, V V, Jose, K A and Kelly, J F, 'Electronically Steerable Leaky-wave Antenna using Tunable Ferroelectric Materials,' *Journal of Smart Materials and Structures*, **3**, 470–475.
88. Varadan, V K and Varadan, V V, (1994). 'Electronically Steerable Automobile Collision Warning Antennas Using Tunable Ferroelectric Materials,' *Wireless Symposium*, Santa Clara, CA.
89. Varadan, V K, Selmi, F and Varadan, V V, 'Voltage Tunable Dielectric Ceramics which Exhibit Low Dielectric Constants and Applications thereof to Electrical Structures,' US Patent (Serial No. 08/260,053) awarded 1996.
90. Lin, L Y, Lee, S S, Wu, M C and Pister, K S J, (1995). 'Micromachined integrated optics for free space interconnection,' *Proc. IEEE MEMS'95*, 77–82.
91. Smith, J H, Montage, S and Sniegowski, J J, (1995). 'Material and processing issues for the monolithic integration of microelectronics with surface-micromachined polysilicon sensors and actuators,' *Proc. SPIE*, **2639**.
92. Markus, K W, et al., (1995). 'MEMS infrastructure: the multiuser MEMS processes (MUMPS),' *Proc. SPIE*, **2639**.
93. Vellokoop, M J, Lubking, G W, Sarro, P M and Venema, A, (1994). 'Integrated-circuit-compatible design and technology of acoustic-wave-based microsecond,' *Sensors and Actuators A*, **44**, 249–263.